Lawrence Berkeley Laboratory
UNIVERSITY OF CALIFORNIA

Materials & Molecular Research Division

THE PLASMA ENHANCED DEPOSITION OF IRON AND IRON OXIDE THIN FILMS

Daniel Mark Wroge
(M.S. thesis)

September 1979

Prepared for the U.S. Department of Energy under Contract W-7405-ENG-48

THE PLASMA ENHANCED DEPOSITION OF IRON AND IRON OXIDE THIN FILMS

Daniel M. Wroge

Lawrence Berkeley Laboratory
University of California
Berkeley, California

Table of Contents

LIST OF FIGURES

Page

Page

THE PLASMA ENHANCED DEPOSITION OF IRON AND IRON OXIDE THIN FILMS

Daniel M. Wroge

Material and Molecular Research Division
Lawrence Berkeley Laboratory
University of California
Berkeley, California 94720

ABSTRACT

Plasma enhanced deposition was used to form iron and iron oxide thin films from an iron pentacarbonyl source in a glow discharge, parallel plate reactor. The carbon and oxygen content of the films increased with increasing rf power. The increase in oxygen content was much greater than that of carbon, however, for films deposited at substrate temperatures above 200°C. Small crystallites (30 - 300Å) of α-Fe and iron oxide (Fe_3O_4 or γ-Fe_2O_3) were formed at substrate temperatures of 150°C or above. The concentration of α-Fe crystallites increased with increasing substrate temperature and appeared to decrease with increasing rf power. Magnetic hysteresis was observed for films deposited at temperatures above 150°C. The coercive force ranged from 5 to 45 oersteds, increasing with both increasing substrate temperature and increasing rf power. The specific magnetization at saturation decreased from 2 to 0.4 weber-meter/kilogram by increasing the rf power from 10 to 100 watts. Square hysteresis loops ($B_r/B_s \approx 1$) were observed for a substrate temperature of 300°C and rf power levels above 30 watts. The magnetization, $\vec{M}$, was found to lie in the film plane.

I. INTRODUCTION

A. Magnetic Thin Films

Magnetic thin films have been of great interest for many years. The large number of applications range from magnetic recording tape to magnetic discs for bulk computer memories to magnetic recording heads, and finally to the more recent magnetic bubble devices.[1-3] A specific application depends strongly upon the magnetic properties of the film weighted against the relative cost and ease of processing. Since the magnetic properties are of prime importance, they will be discussed in more detail below.

A ferromagnetic material such as iron has associated with it a spontaneous magnetic moment even in the absence of an applied magnetic field. This spontaneous moment is due to the parallel alignment of electron spins on neighboring atoms. In some cases an antiparallel spin arrangement is observed. The material is then considered ferrimagnetic. If the magnetic moments exactly cancel, the material is antiferromagnetic (see Fig. 1). The average magnetic moment per unit volume is defined to be the magnetization, $\vec{M}$.

Even though the magnetic moments are aligned on a microscopic scale, the magnetic moment of an entire specimen may be much less than the saturation moment. This is due to the presence of magnetic domains: regions within which $\vec{M}$ is saturated in a given direction but surrounded by other domains with differing directions of $\vec{M}$ (see Fig. 2). The regions bounding the domains are called domain walls. Within these domain walls, the magnetization vector rotates

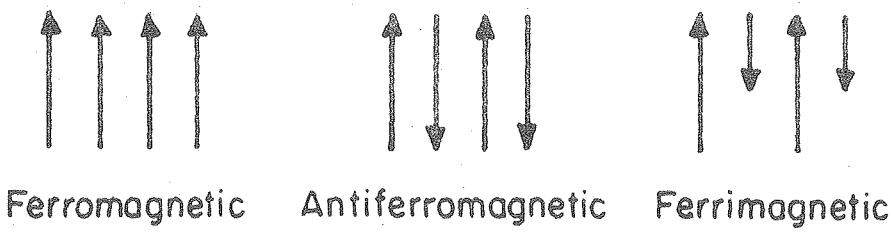

Fig. 1. Ordered arrangement of electron spins in most magnetic materials.

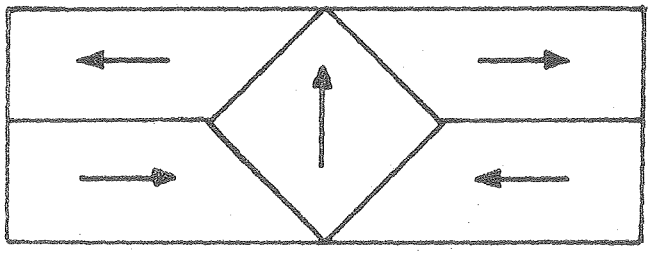

XBL7910-7235

Fig. 2. Variation in direction of the magnetization vector, $\vec{M}$, between domains.

from the direction found in one domain to that found in an adjacent domain.

The application of a magnetic field $\vec{H}$ to a material with magnetization $\vec{M}$, produces a torque on $\vec{M}$ which tends to align it with the applied field. Initially, energy considerations restrict the rotation of $\vec{M}$ to the regions within the domain walls. At sufficiently high magnetic fields the domain walls begin to move, increasing the area of domains favorably oriented with respect to the field at the expense of domains with different directions of $\vec{M}$. As the magnetic field increases, the favorable domains continue to grow. Finally, at large enough field strengths, the domain growth stops and the remaining unfavorably aligned domains rotate into alignment with the applied field. The material is now saturated with respect to the magnetic moment.

The changes in magnetization with applied magnetic field discussed above can be shown by a plot of the magnetization $\vec{M}$ (ampere-turns/meter) or magnetic induction $\vec{B}$ (tesla) versus the magnetic field $\vec{H}$ (ampere-turns/meter). The magnetic induction is defined by

$$\vec{B} = \mu_o (\vec{H} + \vec{M}) \qquad (1)$$

where μ_o is the permeability of free space and has the value 4π x 10^{-7} weber/ampere-meter. Such a plot is called a magnetic hysteresis loop (see Fig. 3). The reverse magnetic field required to bring the magnetic induction to zero is the coercive force, H_c. The saturation induction, B_s, is the limiting form of $\vec{B} - \mu_o \vec{H}$ for large $\vec{H}$. The remanent induction B_r is the magnetic induction at zero applied field. Finally, the saturation magnetization is B_s/μ_o.

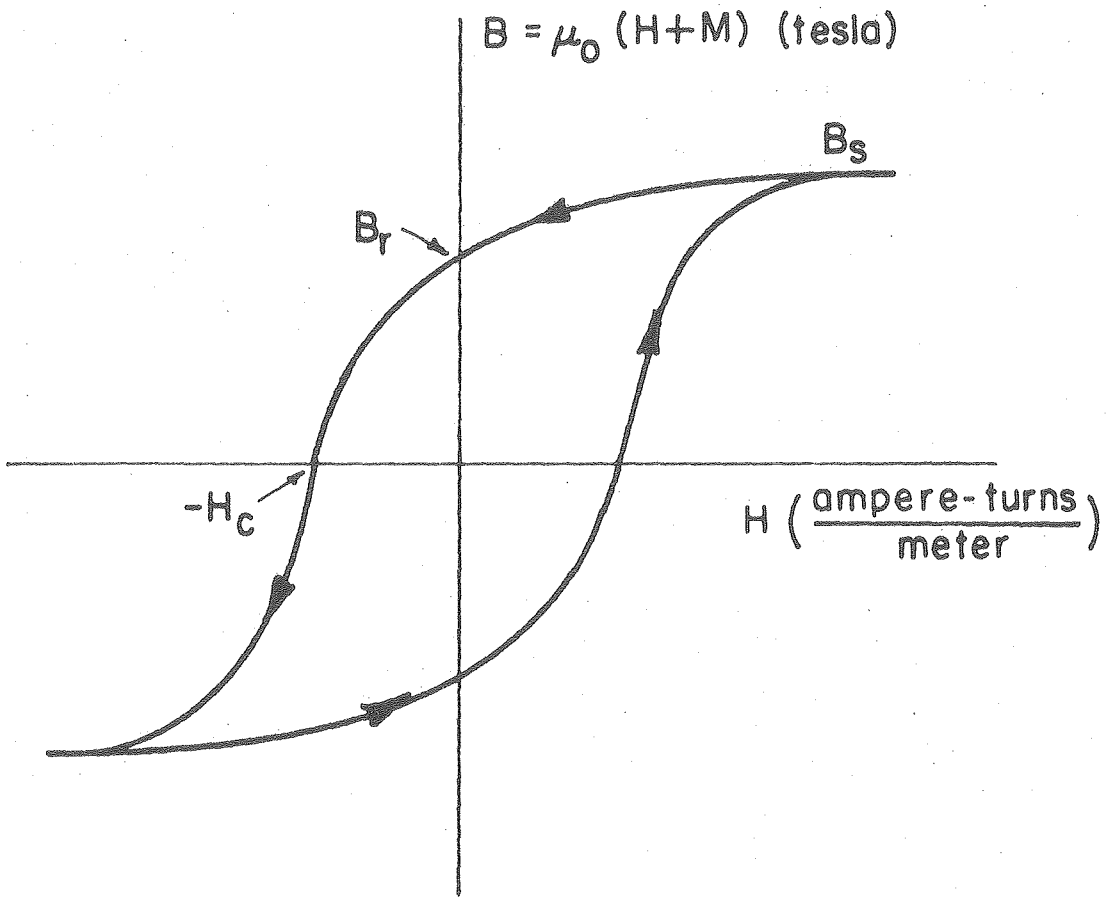

XBL 7910-7236

Fig. 3. Magnetic hysteresis loop. The coercive force is H_c; the remanence is B_r; the saturation induction is B_s (the limiting form of $\vec{B}-\mu_o\vec{H}$ for large $\vec{H}$); the saturation magnetization is B_s/μ_o

The saturation magnetization is a function of the film composition, crystal structure, and the temperature.[40] The coercive force, however, is a function of how difficult it is to move the domain walls. A high coercive force implies an immobile domain wall. An immobile domain wall may be caused by structural defects such as nonmagnetic inclusions, voids, or precipitates of a nonmagnetic phase.[5] Materials consisting of very fine (single domain) grains often exhibit high coercivities as well.[6]

Commercially pure bulk iron has a saturation induction of 2.16 tesla with a coercive force of about 1 oersted,[42] while bulk magnetite (Fe_3O_4) has a saturation induction of 0.61 tesla and a coercive force of 8 - 100 oersted.[43] The wide range observed for the coercive force of magnetite is a result of particle size variation. The coercive force increases as the particle size decreases.

The coercive force and saturation induction vary widely in iron thin films depending upon the amount of film oxidation that has occurred. While pure iron films exhibit a saturation induction close to that of bulk iron, any subsequent oxidation tends to reduce this value.[44] The coercive force of iron thin films has been reported to range from 20 to over 250 oersteds.[45] This increase in coercive force was attributed to an increase in surface roughness or to increasing oxidation in the films.

Since the magnetization of a sample may be "switched" from one direction to another by the application of a strong enough magnetic field, magnetic materials act as excellent memory elements.[4] In addition, the switching speeds of very thin (single domain) magnetic films are

typically on the order of 10^{-9} seconds. The energy loss associated with switching the magnetization from one direction to another is proportional to the area enclosed by the B-H hysteresis loop. For high frequency applications then, small hysteresis losses are essential. This is achieved by obtaining a small coercive force.

Still another problem at high frequencies relates to the fact that fluctuating magnetic fields induce the flow of electrical currents (eddy currents) by Faraday's law. This energy is lost as electrical resistance heating of the magnetic material. Thus at very high frequencies, materials of high electrical resistivity are used to reduce these current losses.

B. Magnetic Film Deposition Methods

In the past, magnetic films have been deposited in various ways.[7,8] The most widely studied technique is that of vacuum evaporation. In this technique, the magnetic properties depend mainly upon the substrate temperature and film composition. The presence of a magnetic field during film deposition may also be used to induce a preferred ordering of the magnetic moments (uniaxial anisotropy) in the direction of the field. Evaporation is severely limited in that substrate temperature, deposition rate, and the application of an external magnetic field are the only variables.

Electrodeposition is certainly the oldest method available for magnetic film deposition. Here metals are deposited onto the substrate (the cathode) by the passage of a current through a suitable electrolyte in an electrolytic cell. The proper selection of bath conditions is still very much of an art however. The bath composition, pH, and

temperature as well as the current density can all affect the magnetic properties of the deposited film. An additional problem involves the fact that electrodeposition is limited to metal on metal films since a conducting substrate is required.

Finally, cathodic sputtering has received a great deal of attention.[9-12] In this technique, the material to be sputtered is made the cathode in an inert gas (Ar or He) glow discharge. Momentum transfer resulting from the bombardment of the cathode by inert gas ions ejects cathode material which then coats the substrates (anode) in the glow discharge system. This complex deposition environment has allowed the production of many useful materials. Virtually any metal can be sputtered under the appropriate glow discharge conditions with a high degree of uniformity and homogeneity. In terms of film composition, sputtering methods are limited to the composition of one target material at any time, or to simple synthetic products as in the reactive sputtering of iron in an oxygen-argon mixture. In order to vary the film composition, additional targets of varying composition must be fabricated.

C. Plasma Enhanced Deposition

Plasma enhanced deposition (PED) has generated considerable recent interest. It has been found that chemical reactions normally requiring high temperatures for thermal activation occur at low and even ambient temperatures by means of plasma enhancement.[13] In addition, the complicated nature of this plasma environment has allowed the formation of compounds with often unique chemical and physical properties.[14-16]

PED, like chemical vapor deposition, offers wide control over film composition since gas streams are used as the reactants. A change in gas composition will directly affect the composition of the film. In addition, PED offers a large number of deposition variables. For example changes in substrate temperature, rf power, gas pressure, rf frequency, gas dynamics, and electrode spacing all may be studied as functions of changing film properties.

PED utilizes a low pressure (13 - 650 Pa) rf electrical discharge. Under these conditions, a large electrical potential is applied between two parallel electrodes causing the ionization of gas species present between the electrodes. The free electrons created are accelerated to high energies by the electric field. Electrons with kinetic energies over 1 eV are capable of producing further ionization of gas molecules, atoms or ions which are present in the system. This in turn produces more electrons. The process continues until a steady-state is attained between electron production and recombination. The degree of ionization is typically 10^{-5} to 10^{-6} with an electron concentration of 10^{10} to 10^{11} cm^{-3}.[17] In addition to ions, however, the electrons are capable of exciting gas molecules to higher electronic states, and forming metastables, free radicals, and atoms which are chemically active. These species are found to be very important in plasma processes since they exist in larger concentrations than ions and often have considerably longer lifetimes.[18] Since the electrons provide energy for chemical activation, processes normally requiring high temperatures may occur at considerably reduced temperatures.

Much work has been done on PED in general,[19,20] yet little work has been done on its application to magnetic thin films. Par Lauriat[21] reported the deposition of amorphous powdered iron films from iron pentacarbonyl and neon in a glow discharge at room temperature. In addition, Secrist and Mackenzie[22] reported the deposition of crystalline γ-Fe_2O_3 at room temperature by the decomposition of iron pentacarbonyl and oxygen in a microwave discharge. The oxide consisted of two phases: a reddish colored phase with an index of refraction greater than 1.70, and a clear phase with an index of refraction of 1.538. The film was identified as a mixture of γ-Fe_2O_3 and Fe_2O_3-H_2O from Debye-Scherrer x-ray powder patterns.

This thesis concentrates on the effects of substrate temperature, rf power, and gas pressure on films of iron and iron oxide deposited in a glow discharge reactor from iron pentacarbonyl source vapor. The film properties investigated are crystallinity, chemical composition, and magnetic hysteresis. The changes in film properties are correlated with changes in deposition conditions.

II. EXPERIMENTAL APPARATUS AND PROCEDURES

A. Equipment

1. Plasma Reactor and Gas Flow System

The plasma reactor and accompanying gas flow system used in this study are shown in Fig. 4. The Pyrex bell jar (10 in diam. x 12 in. in height) enclosed two parallel stainless steel electrodes of 12.7 cm (5 in.) diameter with an electrode spacing of 2.5 cm. The top plate was supported by two alumina tubes and a solid alumina rod. The rf power was supplied by a 0 - 300 watt Tegal rf generator (Model RFG300) and impedance matching network (Model MN300) operating at 13.56 MHz. The system was evacuated through four holes in the central support tube by a Sargent-Welch mechanical vacuum pump (13.6 cfm) and could be ultimately pumped below 2.6 Pa (.02 Torr). The pressure was monitored by a McLeod gauge. The reactor pressure could be varied by changing the pumping speed of the vacuum pump with a throttling valve.

The substrates, normally glass slides or glass cover slips, were placed on the lower electrode and could be heated to 300°C by a nichrome resistance wire attached to the underside of the plate. The temperature was monitored by an iron-constantan thermocouple fed through a hole in the underside of the plate and afixed within 0.065 in. of the electrode surface. As a result of this method of temperature measurement, some discrepancy (<20°C) existed between the actual surface temperature of the substrate and the measured temperature.

Iron pentacarbonyl, a liquid at room temperature with a vapor pressure of 4000 Pa (30 Torr), was stored in a glass flask at room temperature (25°C) and was allowed to evaporate and enter the bell

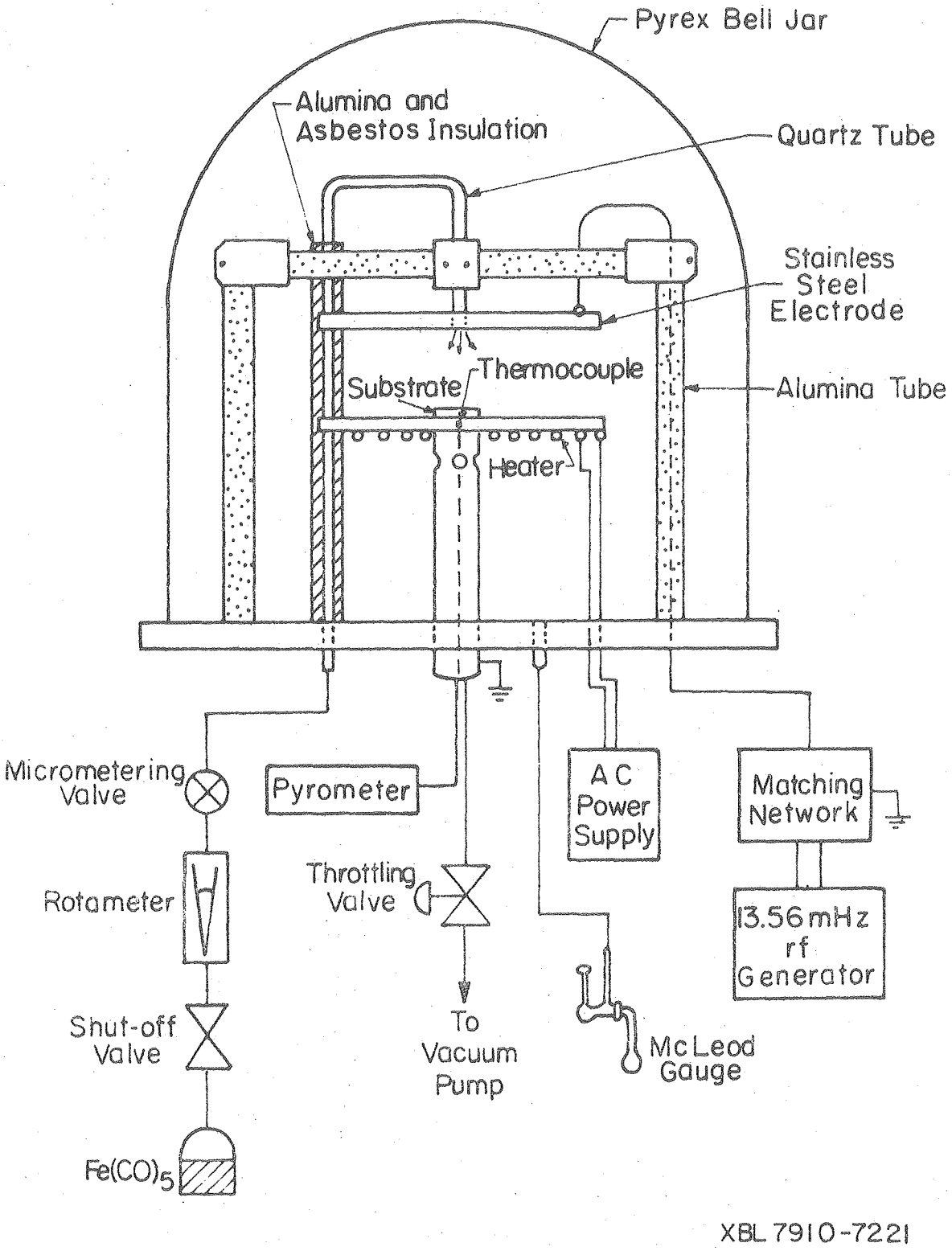

Fig. 4. Glow discharge reactor schematic.

jar chamber through a central hole in the top electrode. The flow was controlled by a shut-off valve, a rotameter, and a micrometering valve (see Fig. 4). A flow rate of 0.015 g/min was always used. This resulted in a typical pressure of 26.6 Pa (.2 Torr). Since iron pentacarbonyl thermally decomposes above 200°C, asbestos tape and an alumina tube insulated the quartz tube as it passed the hot lower electrode.

2. Hysteresis Looper[23-25]

The magnetic hysteresis properties of the deposited thin films were investigated with a hysteresis-looper. A diagram of the apparatus is shown in Fig. 5. The magnetic induction of the sample was displayed as a function of the applied magnetic field on an oscilloscope (Tektronix model 541A).

The sinusoidally varying magnetic field was generated in an eight inch solenoid containing 3470 turns of copper wire (1.29 mm diameter). The inside diameter of the solenoid was 5 cm. The frequency of 150 Hz was the resonance frequency of the RLC network made up of the solenoid (.25 Henry), a capacitor (2 μf), and a resistor (5 ohms). Currents of zero to four amperes through the solenoid generated magnetic fields up to 0.06 tesla. An output voltage proportional to the magnetic field was generated across the resistor in series with the drive coil and was fed to the horizontal plates of the oscilloscope.

Two identical pick-up coils with 2200 turns each of copper wire (.3 mm diameter) were connected in opposition and positioned symmetrically within the solenoid. Since the coils did not cancel exactly, small pieces of aluminum were placed inside of one coil until the output signal was minimized with no sample present. The output was then

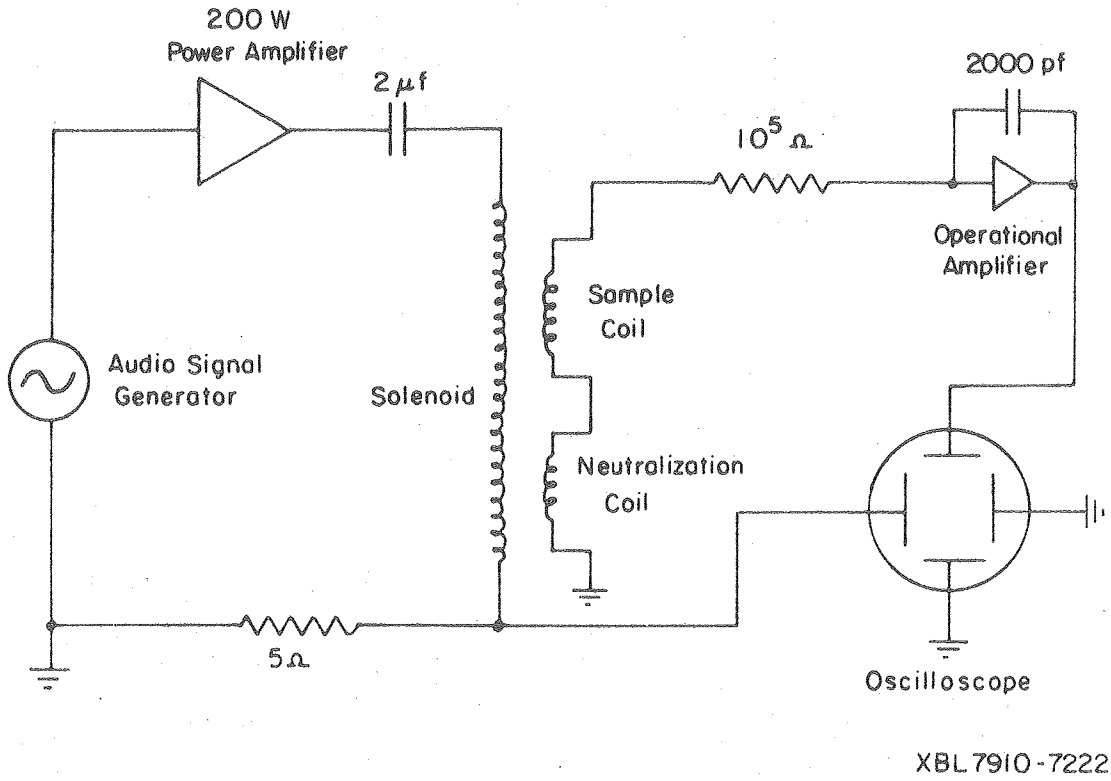

Fig. 5. Hysteresis looper schematic.

fed through a resistor (10^5 ohm) followed by a capacitor (2000 pf) in parallel with an operational amplifier. This amplified and integrated the signal from the pick-up coils. The gain of this amplifier is a function of the RC time constant and the operating frequency. By trial and error, a time constant of 2×10^{-4} seconds was selected, which resulted in a well defined hysteresis loop on the oscilloscope screen. In addition, it was found that a sample mass of at least 3 mg was required to generate sufficient signal from the sample coil. Samples of smaller mass resulted in loops approaching the noise background level.

The vertical scale of the oscilloscope measured directly the flux (ϕ) of the magnetic induction $\vec{B}$ through the cross-sectional area of the deposited film ($\phi = \int_s \vec{B} \cdot d\vec{s}$). The horizontal scale was directly proportional to the magnetic field strength, $\vec{H}$. The horizontal and vertical scales were calibrated by measuring the vertical and horizontal deflections on the oscilloscope screen for a sample with known coercive force and saturation flux.

In order to determine the actual saturation induction, the cross-sectional area of the film was required. For the glass substrates used here, the cross-sectional area was $0.018 \times t$ meter^2, where t is the film thickness. The saturation induction then becomes

$$B_s = \frac{\phi}{0.018 \times t} \qquad (2)$$

Since the film thickness was not known accurately and the density could not be assumed constant, the saturation induction could not be calculated accurately. Instead, the specific magnetization at

saturation (σ_s), defined as the ratio of B_s to the density (ρ), was determined. This quantity can be evaluated in the following manner. Since the thickness of the film is related to the film mass, the total film area (A), and the density (ρ) by

$$t = \frac{\text{mass}}{\rho \times A} \tag{3}$$

we have

$$\sigma_s = \frac{B_s}{\rho} = \frac{\Phi \times 0.018}{\text{mass}} \tag{4}$$

by substitution of Eq. (3) into Eq. (2) and rearrangement.

3. X-Ray Diffractometer[26]

A Picker (Model 3488) x-ray diffractometer was used to study the structural properties of the deposited films. A schematic of this apparatus is shown in Fig. 6. A monochromatic x-ray source (Cu K_α radiation at 1.54Å) was directed onto the sample. The x-rays were then diffracted by the polycrystalline specimen and were detected by a thallium activated NaI detector. The intensity of the diffracted beam was then plotted as a function of twice the incident angle (2θ) on a chart recorder.

A single crystal sample diffracts x-rays according to the Bragg law

$$2d \sin\theta = \lambda \tag{5}$$

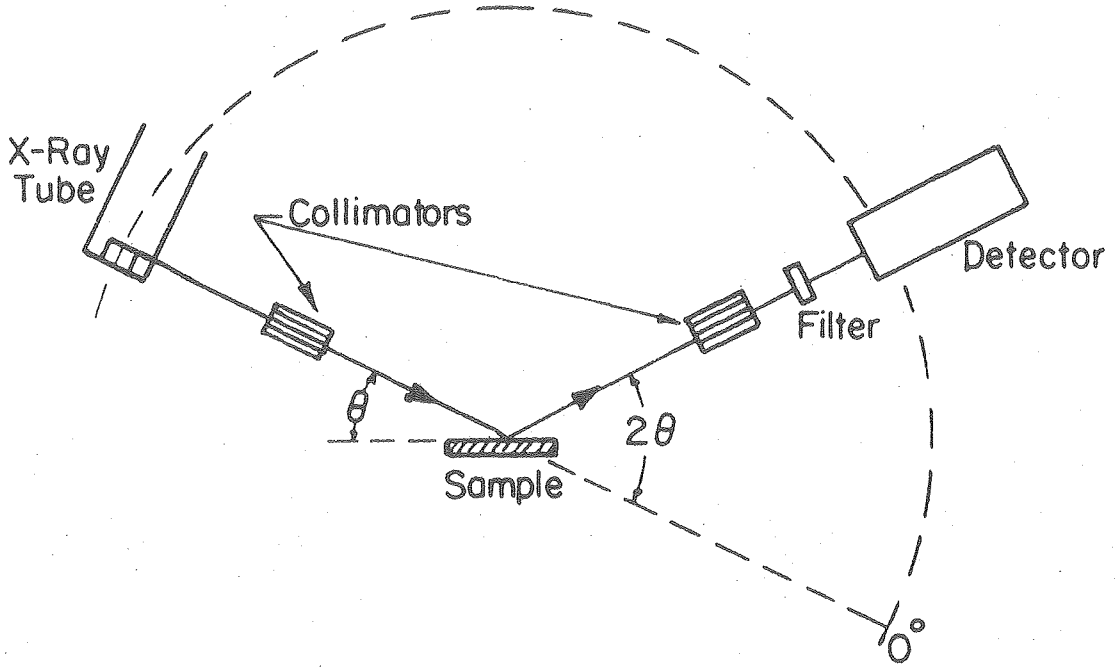

Fig. 6. Schematic of an x-ray diffractometer.

where d is the interplanar spacing, λ is the wavelength of the incident x-rays, and θ is the angle of diffraction. Since the wavelength λ and the diffraction angle θ are known, the interplanar spacing for a single crystal or polycrystalline film can be calculated. The x-ray diffraction patterns for most materials of interest have been published.[27] In Ref. 27, the relative peak intensities versus the interplanar spacings (d) have been recorded for the most intense (hkl) reflections. In this way the intensity of the observed peaks may be compared directly to known samples and a qualitative identification made.

4. Chemical Analysis[28]

The thin films were chemically analyzed for iron and carbon.* The iron content was determined by atomic absorption spectrometry after dissolving the sample in sulfuric acid. The carbon content was determined by a combustion technique where the sample was heated to a high temperature (850°C) in the presence of oxygen and a helium carrier gas. The amount of carbon evolved as CO_2 was then determined by gas chromatography. The oxygen content was determined by difference assuming the samples contained only carbon, oxygen, and iron.

B. Experimental Procedure

Iron deposits were made under a wide range of substrate temperatures, rf power levels, and pressures. For a standard deposit a 1.8 cm x 1.8 cm x .2 mm glass cover slip was used. The substrates were initially

*All analyses were done by the Analytical Chemistry Laboratory in the Department of Chemistry, University of California, Berkeley.

cleaned by a trichloroethylene rinse followed by an isopropyl alcohol rinse and finally they were dried in a dried and filtered nitrogen stream.

Since iron pentacarbonyl thermally decomposes above 200°C care was required to prevent the thermal decomposition at the gas outlet in the upper electrode when substrate temperatures above 200°C were used. The upper electrode was initially removed, the micrometering valve in the iron pentacarbonyl gas line was opened fully, and the reactor was evacuated with the vacuum pump. Current was then supplied to the heating coil to slowly heat the lower electrode. When the desired temperature was reached, the reactor was vented to the atmosphere and the upper electrode, now at room temperature, was replaced and the substrate centered beneath the gas inlet port. The bell jar was replaced and the system was again evacuated.

The substrate was allowed to equilibrate in temperature with the lower electrode for several minutes while the reactor was eventually pumped down to a pressure of less than 2.6 Pa (.02 Torr). The rf power was then turned on as the shut-off valve was opened and the micrometering valve set at a preselected value (see Fig. 4). After the appropriate deposition time, the shut-off valve and micrometering valve were closed, and the system was evacuated for 1 minute. The rf power was then turned off, the reactor was vented to the atmosphere, and the substrate was removed. If a higher operating pressure was desired, the pumping speed of the vacuum pump was reduced by closing the throttle valve.

III. RESULTS AND DISCUSSION

A. General Film Properties

The plasma deposited iron and iron oxide thin films were found to be highly reflective under all deposition conditions. They also demonstrated excellent adhesion to the glass substrates as evidenced by the "Scotch-tape"[49] test under normal thicknesses. However, at very low power levels (<20 watts), the films cracked and curled away from the substrate when the deposits were too thick (>3 μm). This phenomenon is well known in sputtered or evaporated iron films and is normally attributed to tensile stress in the films.[29,30]

Since iron pentacarbonyl thermally decomposes at temperatures above 200°C a direct comparison was made between the plasma enhanced deposits and the deposits resulting from the thermal decomposition of the iron pentacarbonyl vapor. Figure 7 shows a deposit obtained by the thermal decomposition of iron pentacarbonyl at a substrate temperature of 300°C versus a plasma enhanced deposit run at 30 watts rf power and 100°C. While the plasma enhanced deposit was highly reflective, uniform, and adherent, the thermally decomposed iron pentacarbonyl resulted in a non-reflective, powdery deposit which was easily scraped off of the substrate.

The formation of a powdery deposit suggests gas phase nucleation of small particles which subsequently settle onto the substrate. This is in direct contrast to the plasma enhanced deposit where the nucleation and growth of the film appeared to occur on the substrate surface resulting in reflective, uniform films. Such results suggest that any particles formed homogeneously may be dissociated by the

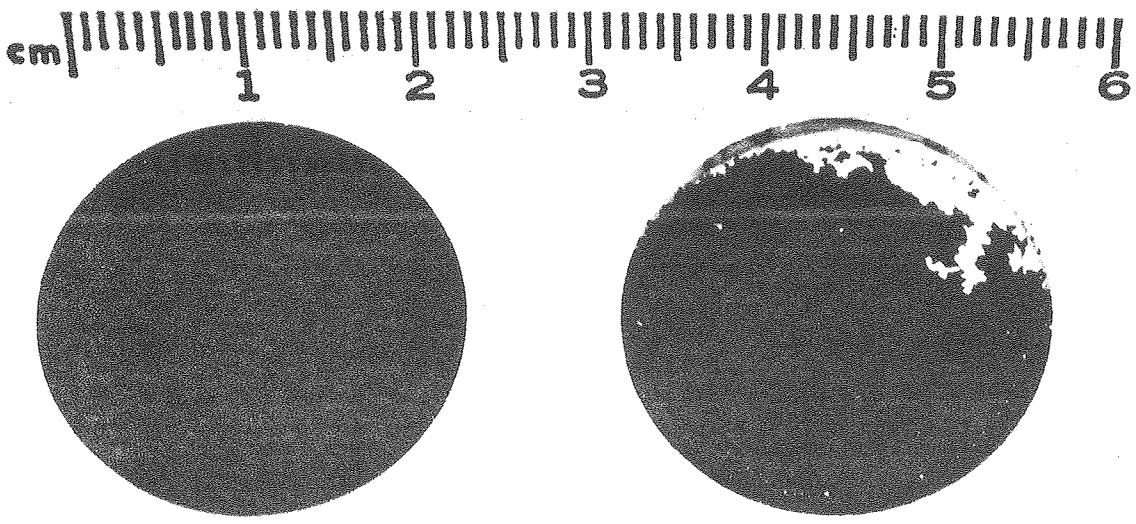

CBB 780-15846

Fig. 7. Films resulting from the plasma enhanced deposition of $Fe(CO)_5$ at 100°C, 30 watts rf power (left) versus the thermal decomposition of $Fe(CO)_5$ at 300°C (right).

collisional processes in the gas plasma, thereby forcing the heterogeneous processes to dominate, and thus precluding powdery deposits.

The thickness of the deposits decreased markedly with radial distance from the center of the electrode. Since the iron pentacarbonyl inlet was located in the center of the upper electrode, these results are not surprising. However, the radial thickness dependence was also a strong function of rf power level. As the rf power increased, the deposit became confined to a smaller area (see Fig. 8). Thus, the probability of decomposition increased with increasing power level, resulting in nearly complete reaction at high power levels as the vapor emerged from the inlet port. For this reason, small substrates centered beneath the gas inlet were necessary under high power conditions.

For the 1.8 x 1.8 cm glass substrates used, the deposition rate was found to be relatively independent of temperature and power (see Fig. 9). Since $Fe(CO)_5$ has an activation energy for decomposition of 0.87 eV,[31] and the average energy of electrons in rf glow discharges at 1 torr is approximately 10 eV, these results are quite reasonable. The slight decrease in the deposition rate at high temperatures was probably a result of the thermal decomposition of iron pentacarbonyl at the inlet port due to heating of the upper electrode during the deposition run.

B. Chemical Composition

The iron/iron oxide films were chemically analyzed (see Section II.A.4) for iron and carbon content under a wide range of substrate temperatures and rf power levels. The oxygen content in the films was determined by difference assuming the films to be composed entirely

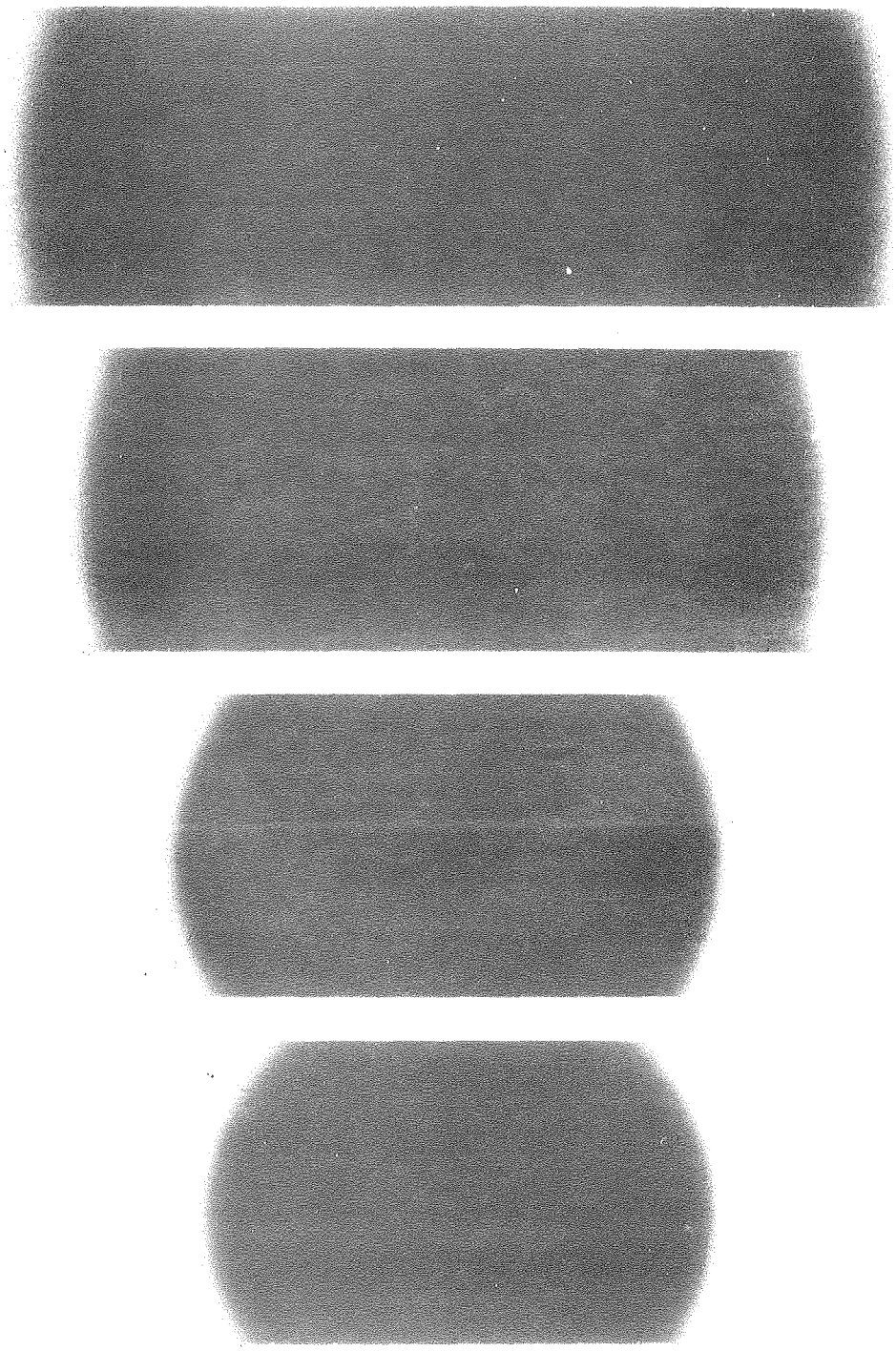

Fig. 8. The radial thickness dependence of iron/iron oxide films versus the rf power level at a substrate temperature of 250°C (10 watts (top), 20 watts, 50 watts, and 100 watts (bottom)). The darkened regions of the glass slides represent a relatively constant thickness of about 1.5 microns.

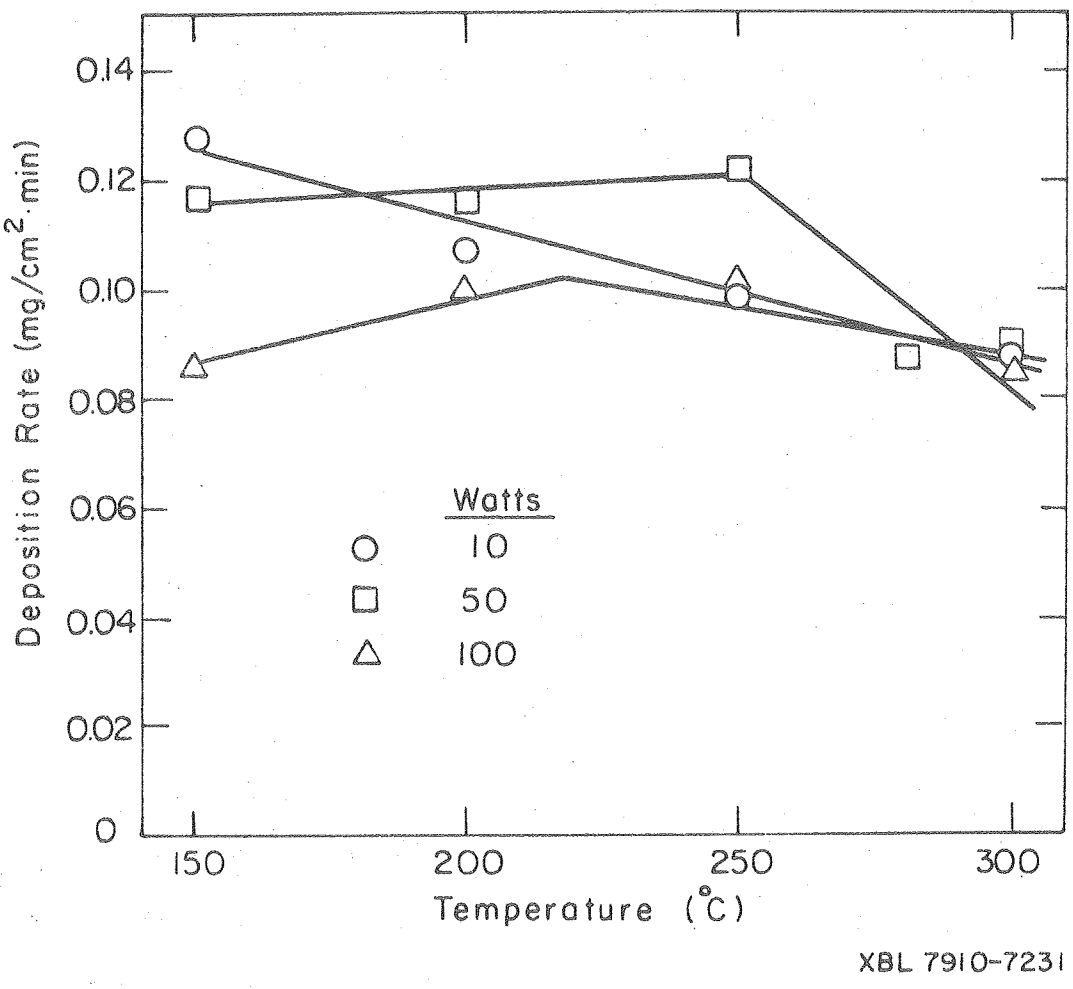

Fig. 9. The deposition rate of iron/iron oxide films versus the substrate temperature.

of carbon, oxygen, and iron. Since the source gas, iron pentacarbonyl, consisted only of iron, carbon, and oxygen this is a reasonable assumption. The results of these analysis are plotted in Figs. 10-12. A marked decrease was observed in iron content as the rf power was increased. This decrease corresponded directly to an increase in oxygen content since the mole fraction of carbon remained approximately constant at 0.10. The oxygen content also increased as the substrate temperature was reduced.

Trends in these data are more obvious if the stoichiometry of the films is considered under the assumption of a constant iron content, and the results are given in Table I. The ratio of the number of moles of carbon to iron and oxygen to iron both increased as the rf power was increased. In addition, the oxygen to iron ratio decreased as the temperature was increased. No definite trend was observed in the carbon to iron ratio as a function of the temperature. The ratio of the number of moles of oxygen to carbon, however, increased as the rf power increased and decreased as the temperature was increased.

The above data suggest that iron pentacarbonyl initially dissociates into iron and carbon monoxide since it is such an unstable compound.[31] As the iron begins to condense onto the substrate, the carbon monoxide may be further dissociated into elemental oxygen and carbon.* The extent of the dissociation of CO will be dependent upon the rf power level. As the power is increased, more elemental carbon

---

*This dissociation of carbon monoxide into elemental carbon and oxygen in a glow discharge is well known. See for example Brown[32] or McTaggert.[33-34]

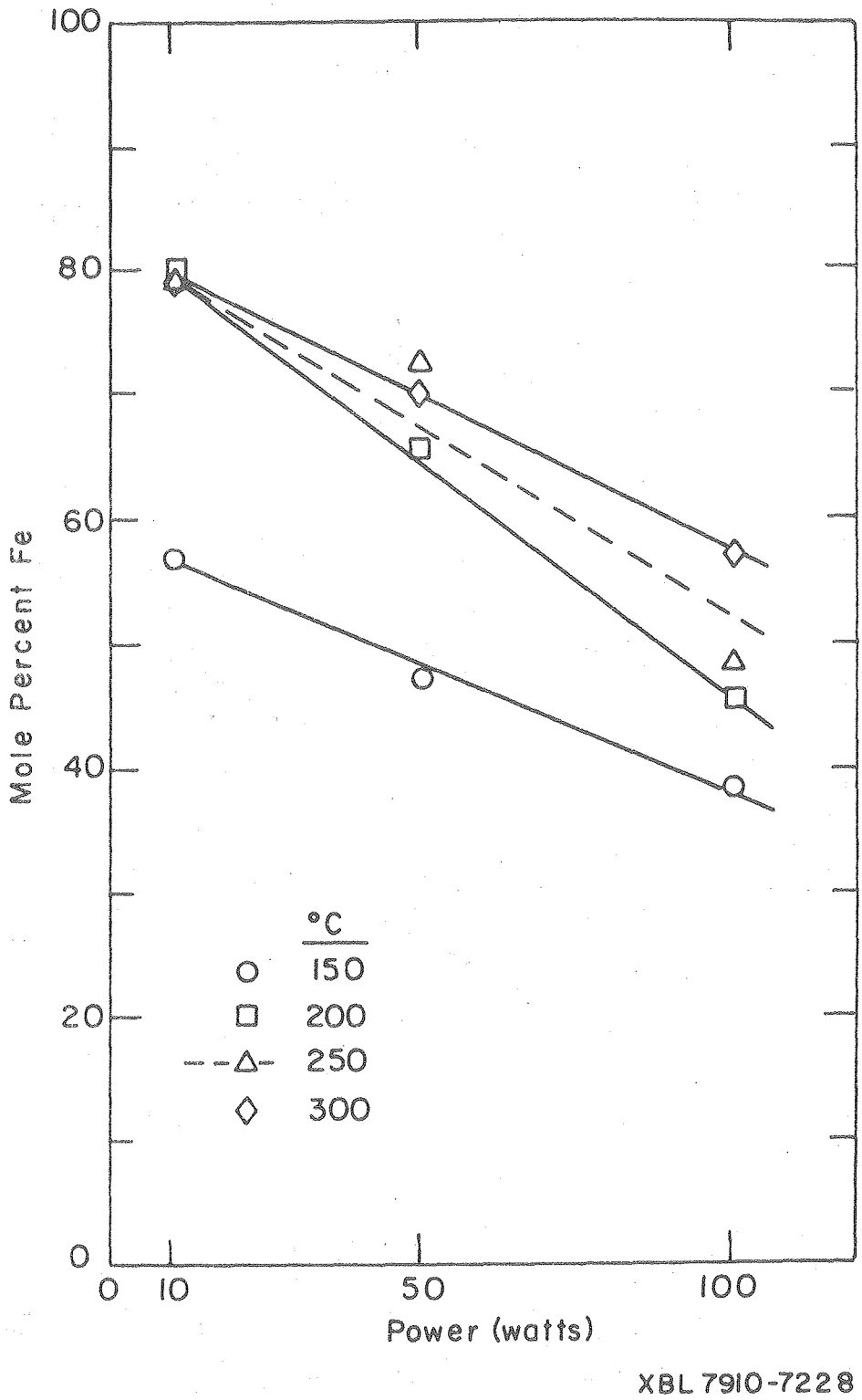

Fig. 10. The mole percent of iron in the films versus the substrate temperature and rf power level.

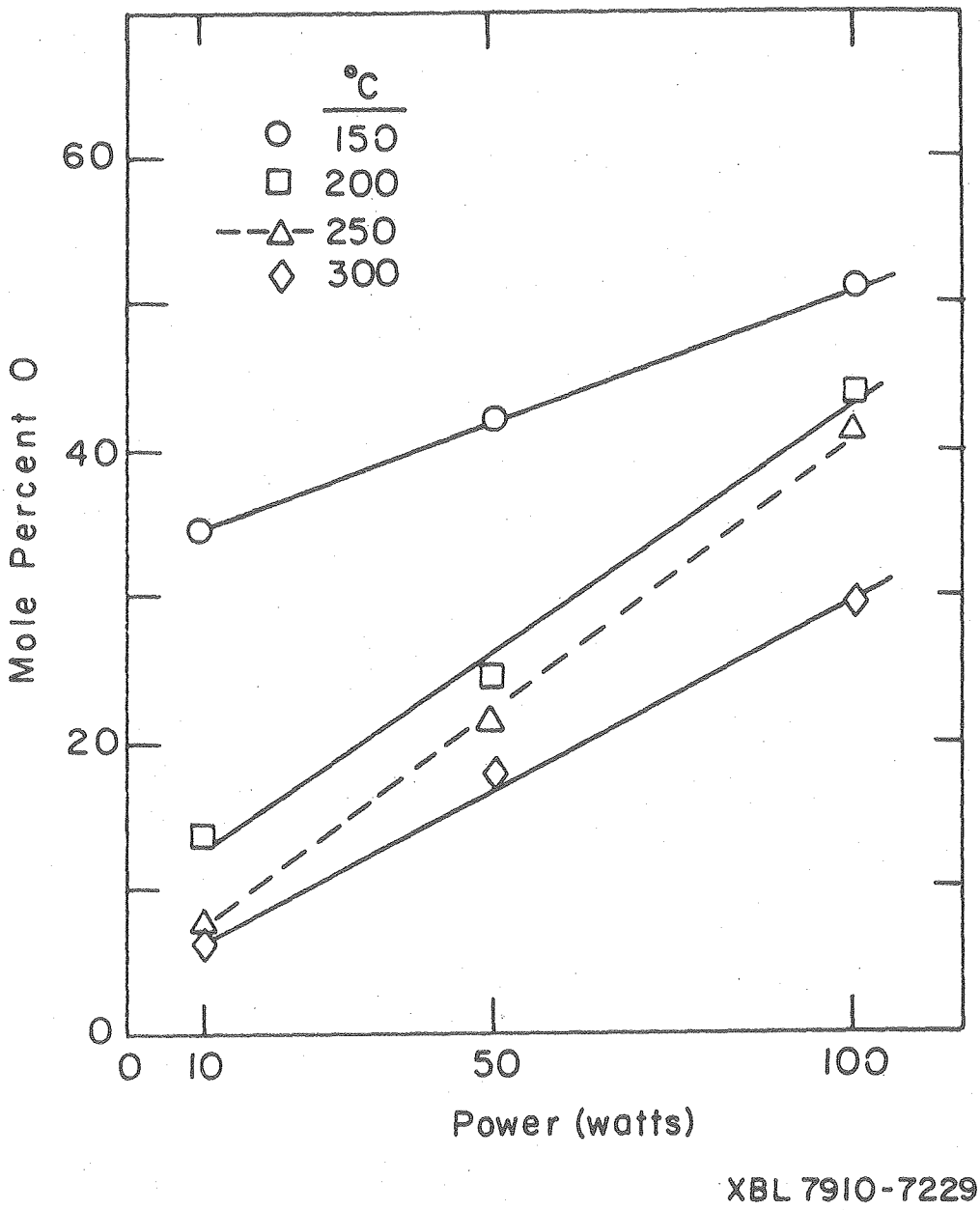

Fig. 11. The mole percent of oxygen in the films versus the substrate temperature and rf power level.

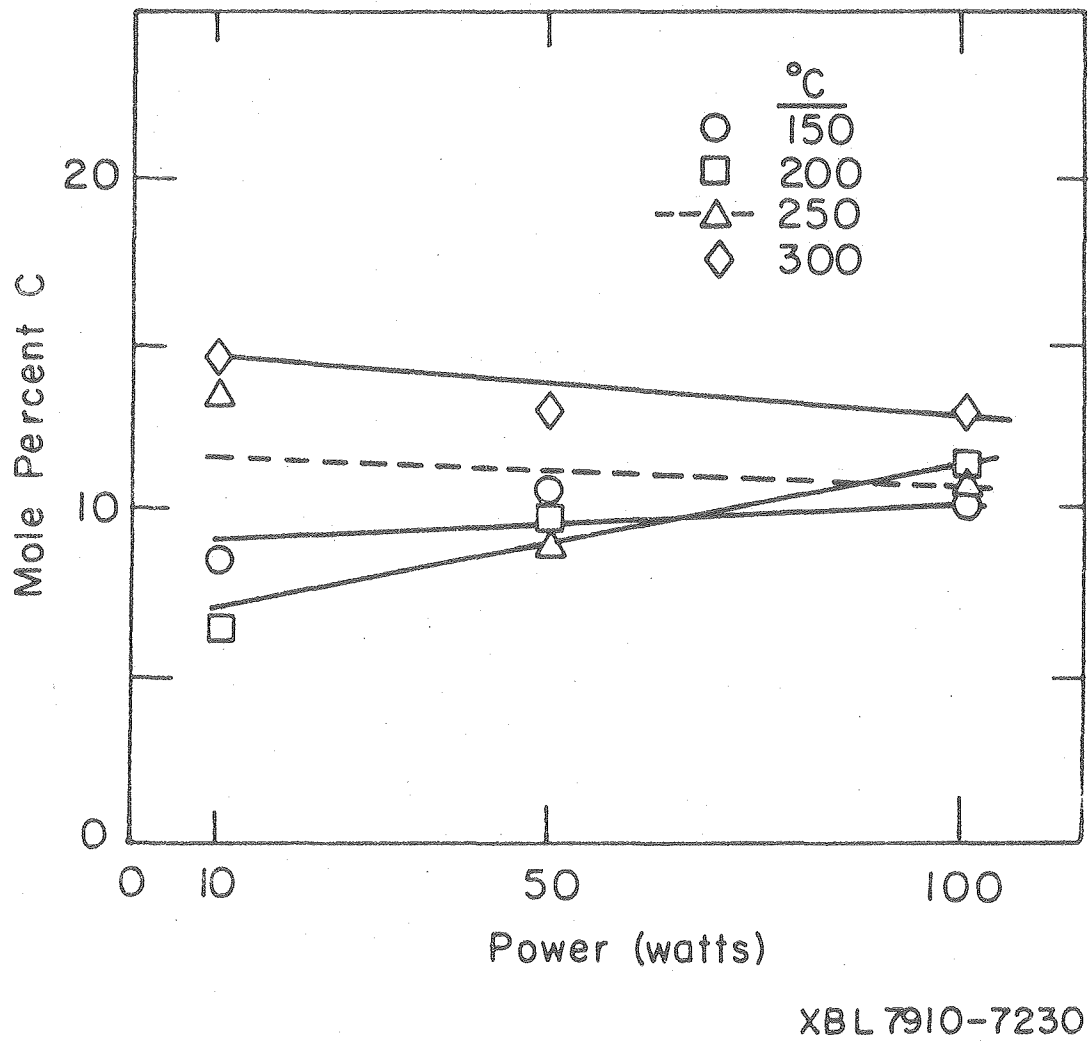

Fig. 12. The mole percent of carbon in the films versus the substrate temperature and rf power level.

Table I. Effect of substrate temperature and rf power level on the film stoichiometry.

Substrate Temperature (°C)	RF Power Level (watts)	Film Stoichiometry	Moles O / Moles C
150	10	$FeO_{.61}C_{.15}$	4.07
150	50	$FeO_{.90}C_{.22}$	4.09
150	100	$FeO_{1.32}C_{.27}$	4.89
200	10	$FeO_{.17}C_{.08}$	2.12
200	50	$FeO_{.38}C_{.15}$	2.53
200	100	$FeO_{.96}C_{.25}$	3.84
250	10	$FeO_{.10}C_{.17}$	0.59
250	50	$FeO_{.27}C_{.12}$	2.19
250	100	$FeO_{.85}C_{.22}$	3.86
300	10	$FeO_{.09}C_{.18}$	0.50
300	50	$FeO_{.25}C_{.19}$	1.31
300	100	$FeO_{.52}C_{.23}$	2.26

and oxygen will be formed. Since a carbon to oxygen ratio of unity was never observed, it is evident that some carbon monoxide present was always dissociated by the plasma. The large increase in the oxygen to carbon ratio with increasing rf power, especially at high temperatures, reflects the high affinity of iron for oxygen at elevated temperatures. This formation of iron oxide at high temperatures and high power levels will be discussed later in terms of the x-ray diffraction data.

The large increase in oxygen content without a corresponding increase in carbon content accompanying an increase in rf power may also be explained in part by considering a black colored powdery residue deposited on the bell jar walls after a deposition run . With the lower electrode heated to 250°C this residue was found to have a stoichiometry of $FeO_{1.55}C_{.35}$ at 10 watts, $FeO_{1.55}C_{.40}$ at 50 watts, and $FeO_{1.60}C_{1.05}$ at 100 watts. Thus, a significant increase in carbon content was observed in this residue as the rf power was increased. This agrees with the observation by McTaggart of a carbonaceous residue that formed on the walls of a reactor which contained a carbon monoxide glow discharge. At very low power levels a partially polymerized orange-red carbon suboxide C_3O_2 was formed according to the mechanism shown below.[33]

$$CO + e \rightarrow CO^* + e \qquad (6)$$

$$CO^* + CO \rightarrow C_2O + O \qquad (7)$$

$$C_2O + CO \rightarrow C_3O_2 \qquad (8)$$

where CO^* designates an electronically excited CO molecule. As the power was increased a dark residue of empirical composition $CO_{.78}$ formed, while at even higher power levels thick, soft layers of carbon were formed on the walls of the discharge tube.[34]

The reduction in oxygen content with increasing temperature is more difficult to explain. These observations could be attributed in part to a desorption phenomenon of a species such as CO or O_2 at elevated temperatures. The preferred desorption of O_2 would explain why a much greater reduction in oxygen content occurs in comparison to that for carbon. A more detailed study must be made into the processes occurring in the plasma as a function of substrate temperature and rf power before any more definite conclusions can be drawn concerning the actual processes involved.

C. Film Structure

1. X-Ray Diffraction Results and Discussion

The x-ray diffractometer described in Sec. II.A.3. was used to study the crystallinity of the deposited thin films. The x-ray diffraction patterns verified the polycrystalline nature of the deposits. The intensity of various diffraction peaks varied widely depending upon the substrate temperature and rf power level. Since the films consisted only of iron, oxygen, and carbon the diffraction patterns were compared to those recorded for iron, the iron oxides, and the iron carbides.[27] The characteristic peaks of the iron carbides were not observed indicating that the carbide phases either do not form or form to only a small extent. Three peaks located at 2θ values

of 45, 83, and 65 degrees (Cu Kα radiation) with relative intensities 100, 20, 10 agree with those recorded for the alpha phase of iron (44.6, 82.3, 65.2 degrees with relative intensities 100, 30, and 20 respectively). At high rf power levels and high temperatures small peaks also appeared at 2θ values of 36 and 62 degrees with relative intensities of 100 and 40. These could correspond to either magnetite (Fe_3O_4) (35.5, 62.2, 30.1 degrees with relative intensities 100, 40, 30) or maghemite (γ-Fe_2O_3) (35.6, 62.7, 30.3 degrees with relative intensities 100, 53, and 34). The peak observed at 62 degrees was very small so that the absence of a resolvable peak at 30 degrees is not surprising.

The three iron oxides Fe_3O_4, γ-Fe_2O_3, and α-Fe_2O_3 may all be formed in iron thin films in relative amounts depending upon the temperature.[35-37] A surface layer of α-Fe_2O_3 was reported overlying either Fe_3O_4 at temperatures above 250°C or γ-Fe_2O_3 at temperatures below 200°C.[36] The most intense α-Fe_2O_3 peak at 33 degrees was not observed in the diffraction patterns recorded in this study. However, the absence of the 33 degree peak may be due to the fact that a very thin surface layer may not be able to diffract sufficient x-rays to be detected by the equipment used.

The diffraction patterns observed for the films between 2θ values of 32 and 48 degrees are shown in Figs. 13-16. The most intense peaks for α-Fe (45 degrees) and Fe_3O_4 or γ-Fe_2O_3 (36 degrees) both lie within this region. At temperatures below 150°C no diffraction patterns were observed. The absence of diffraction peaks under these deposition conditions may be due to small crystallites or to a completely amorphous

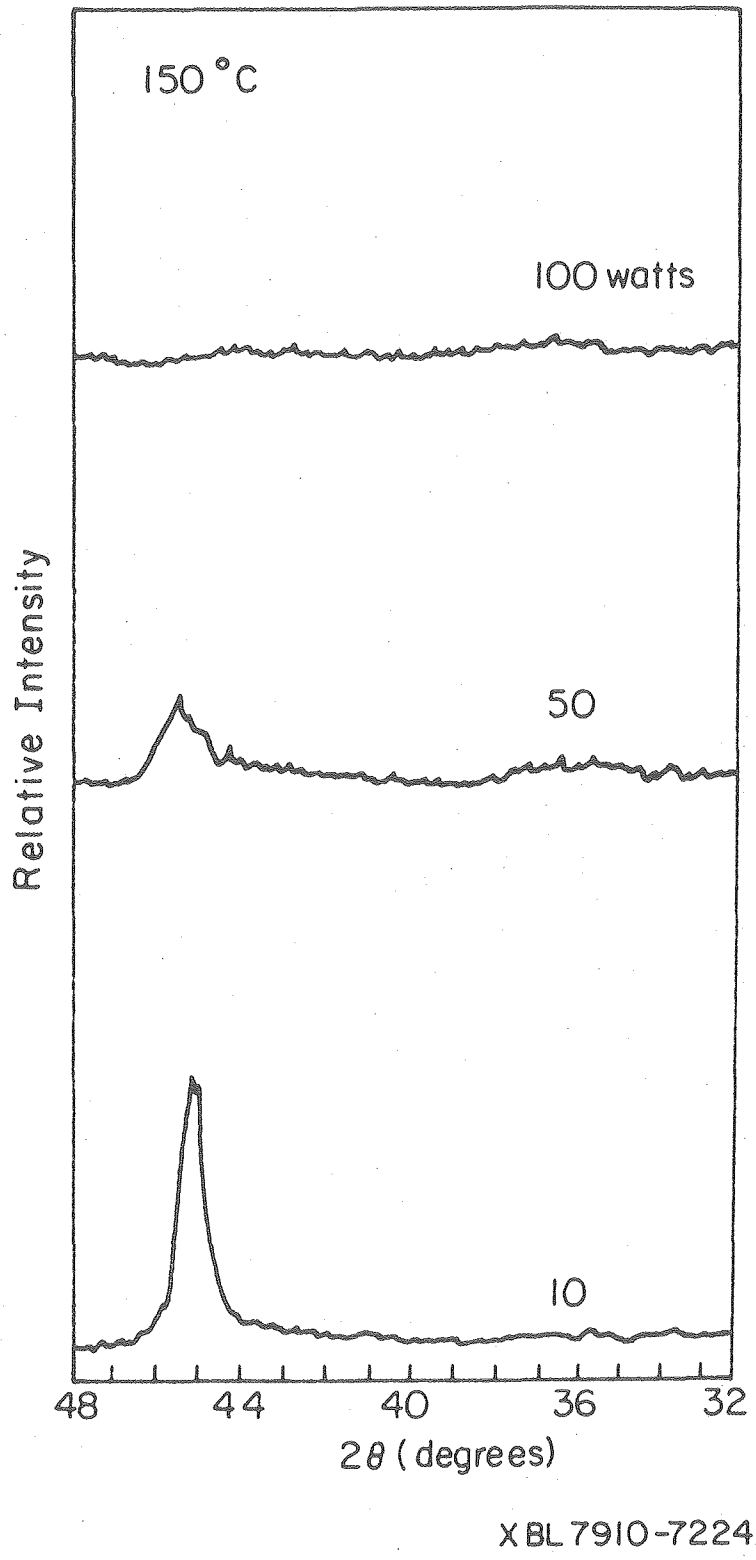

Fig. 13. The x-ray diffraction patterns observed for films deposited at 150°C versus the rf power level.

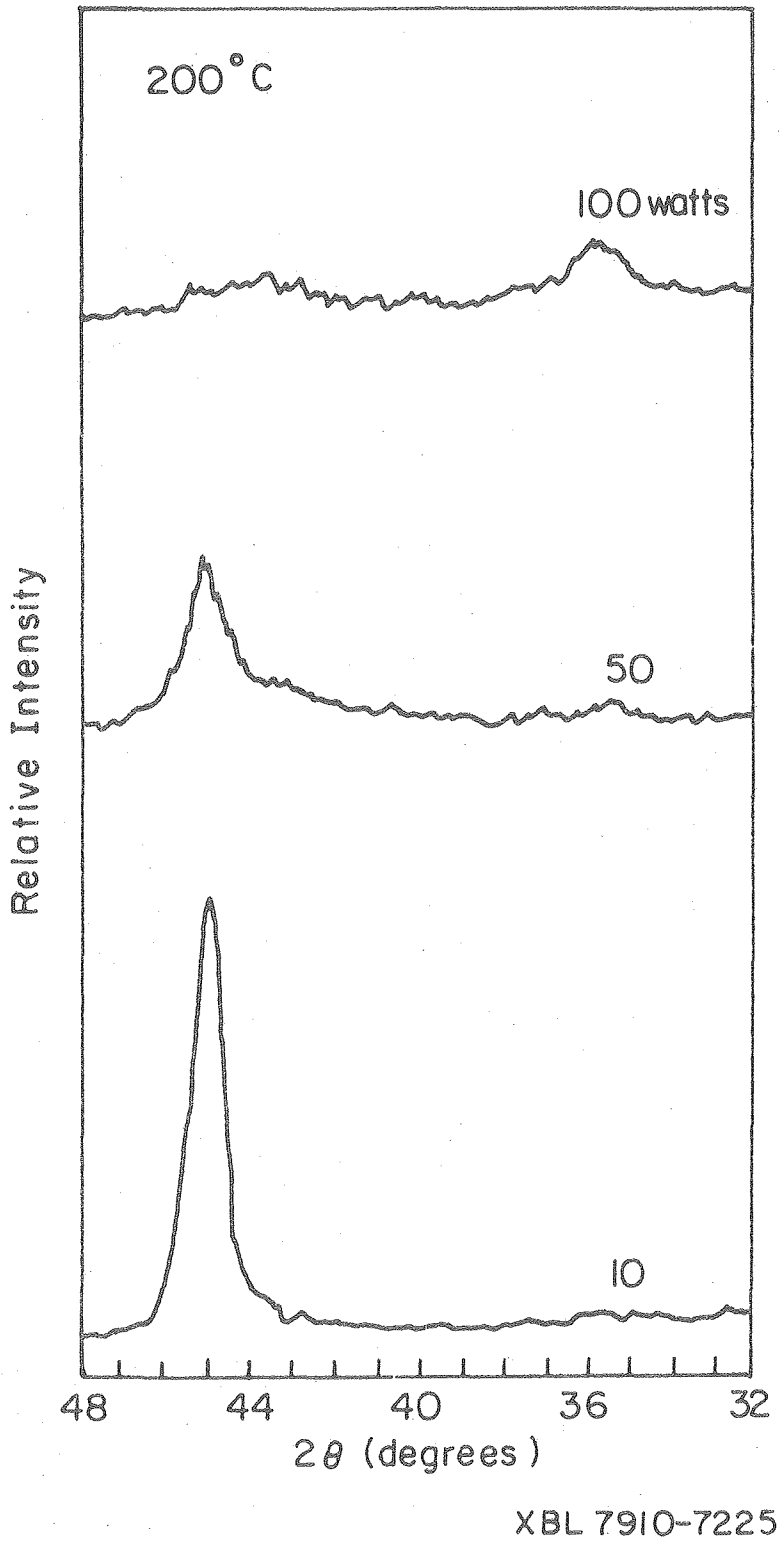

Fig. 14. The x-ray diffraction patterns observed for films deposited at 200°C versus the rf power level.

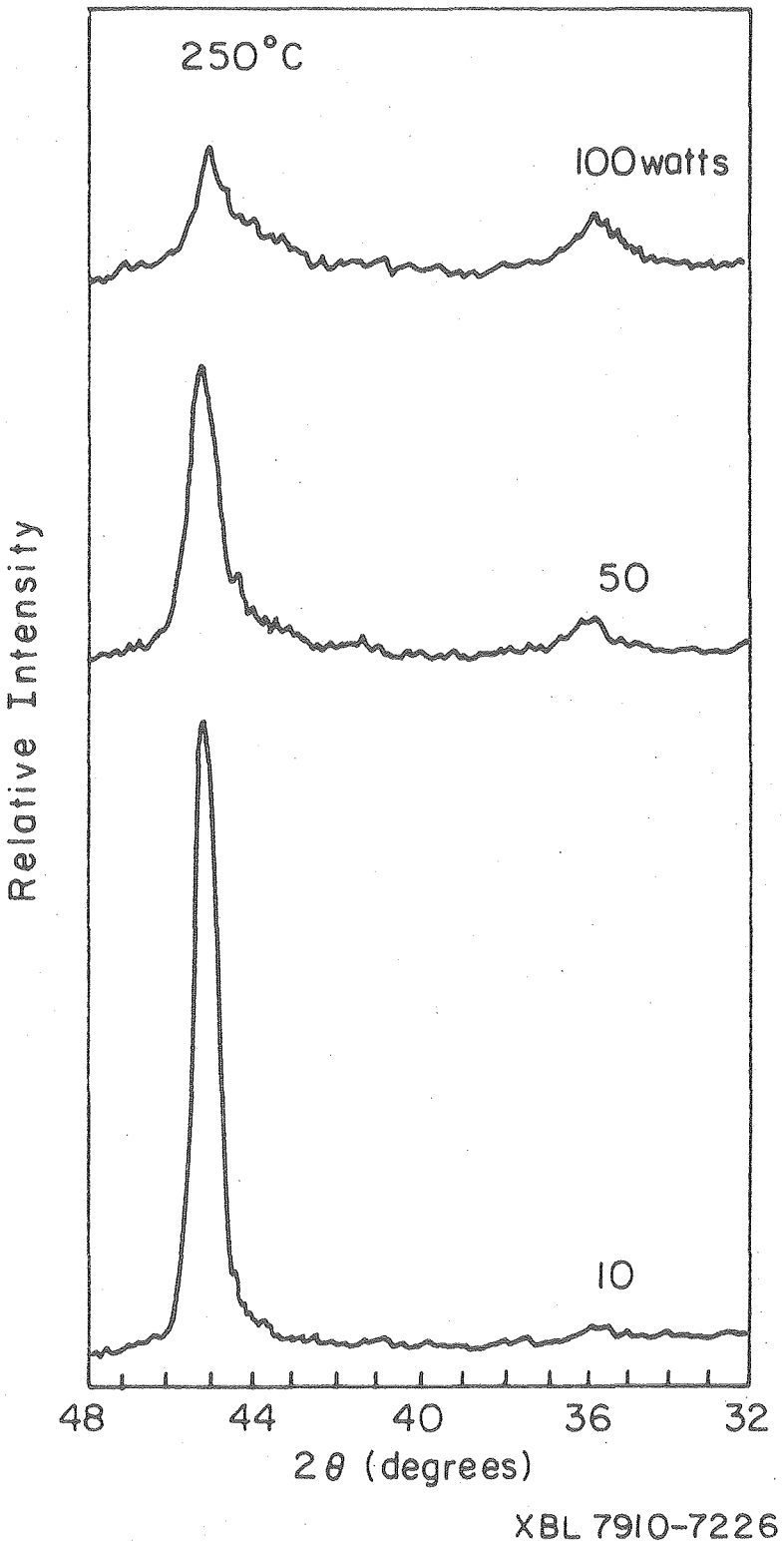

Fig. 15. The x-ray diffraction patterns observed for films deposited at 250°C versus the rf power level.

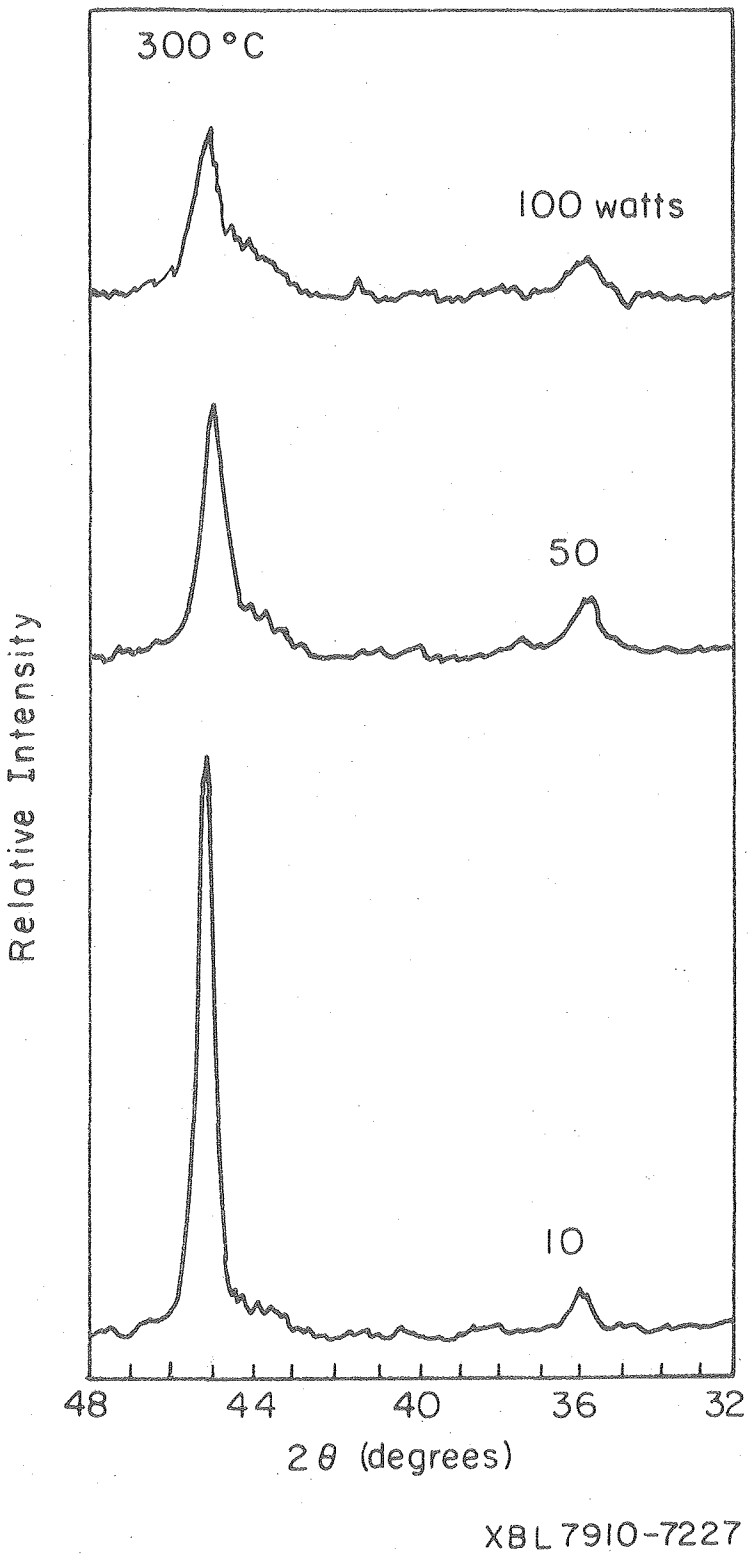

Fig. 16. The x-ray diffraction patterns observed for films deposited at 300°C versus the rf power level.

structure. This will be discussed further in Sec. III.C.2. At temperatures of 150°C and greater, however, a peak was observed at 2θ of 45 degrees. This peak decreased in intensity as the rf power was increased and increased in intensity as the temperature was increased. At 150°C and 100 watts rf power no peaks were observed.

A peak at 36 degrees did not appear until a substrate temperature of 200°C was reached at an rf power level of 100 watts. This peak increased in intensity as the power was increased and increased slightly with increasing temperatures.

The integrated intensity of an x-ray diffraction peak may be affected by a preferred ordering of the crystals, by extinction, or by a reduction in crystallinity.[38] Preferred orientation occurs when the crystals making up the specimen are not randomly distributed but favor some particular orientation. PED, like sputtering, should result in a random distribution of crystals since the reactive species impinge upon the depositing surface in a random manner.

Extinction is due to an increase in grain size or to the growth of large mosaic blocks. As a specimen becomes more perfect, approaching a single crystal arrangement, it has less reflecting power and the peak intensity decreases. An increase in grain size would be expected at higher substrate temperatures since the impinging atoms possess greater kinetic energy thereby allowing significant surface diffusion of the atoms and increasing the probability of attaining a lattice position. These factors predict a reduction in intensity with increasing temperature and this reduction was not observed.

An increase in grain size should also affect the lineshape if some broadening was present initially due to a very small particle size. This broadening mechanism vanishes for a particle size above approximately 1000Å. Since the width of the diffraction peaks at half-maximum remain approximately constant, little can be said about the particle size. The fact that a half-width of almost one degree was observed implies that some broadening mechanism was present, however.

Since the change in intensity of the diffraction peak at 45 degrees does not appear to be due to extinction or to a preferred orientation it was probably the result of an increase in the concentration of iron crystals at increasing substrate temperatures and reduced rf power levels. This conclusion will be discussed further in Sec. III.C.2.

An increase in the amount of crystalline material with increasing temperature indicates that more of the depositing atoms acted as nucleation sites for additional crystal growth when the temperature was increased.

It is well known that an increase in rf power level in glow discharges leads to an increase in surface damage by enhanced electron and ion bombardment.[39] An increase in rf power was also accompanied by a marked reduction in iron content (see Fig. 10). Further, this trend was accompanied by a significant increase in oxygen content. Not only was the concentration of iron reduced but some iron was also consumed in the form of iron oxide. The loss in intensity of the diffraction peak at 2θ of 45 degrees at increasing rf power levels was probably due to both increasing radiation damage from the plasma and to a reduction in the concentration of iron in the film itself.

The x-ray diffraction peak at 2θ of 36 degrees (iron oxide) first appeared at 200°C and 100 watts power. As the temperature continued to increase the peak appeared at reduced power levels; 50 watts at 250°C and 10 watts at 300°C. The increase in rf power was accompanied by an increase in oxygen content (see Fig. 11). An increase in the intensity of the oxide peak with increasing power correlates well with the increase in oxygen content of the films and with the reduction in intensity of the α-Fe peak. A larger activation energy seems to exist for the formation of this oxide in comparison to α-Fe. Higher substrate temperatures are therefore required to produce the iron oxide crystals than were necessary for the formation of α-Fe crystals.

2. Structure From Transmission Electron Microscopy

In order to determine the microscopic structure of the plasma deposited films, three samples were prepared and examined by transmission electron microscopy (TEM).* The samples were deposited onto sodium chloride crystals at 200°C and 30 watts power, 300°C and 10 watts power, and 300°C and 100 watts power. The deposits cracked and bubbled after the substrates were cooled.

In comparison to a coefficient of linear thermal expansion of about $11 \times 10^{-6}\ ^{o}C^{-1}$ for Fe or Fe_3O_4, glass (Pyrex) has an expansion coefficient of $3.2 \times 10^{-6}\ ^{o}C^{-1}$ while that of NaCl is $41 \times 10^{-6}\ ^{o}C^{-1}$.[51] Thus, the contraction of the NaCl upon cooling was much greater than the contraction of the glass cover slips. This explains why the

*TEM experiments were done by Dr. R. K. Mishra in the Department of Material Science, University of California, Berkeley.

deposits cracked readily on NaCl, while under the same conditions they did not crack on the glass cover slips.

Small pieces of the cracked deposits were removed and were subsequently thinned by ion milling[50] to a thickness of about 2000Å. The samples were then examined in a Philips EM-301 electron microscope operating at 100 keV. The dark and bright field images as well as the electron diffraction patterns for the three specimens are shown in Figs. 17-19.

The most intense ring appearing near the center of the electron diffraction patterns corresponds to the (110) reflection of α-Fe. Rings also appeared within this (110) ring. These less intense rings correspond to either Fe_3O_4 or γ-Fe_2O_3. Since the lattice constants and crystal structures of Fe_3O_4 and γ-Fe_2O_3 and so similar, the actual form of iron oxide present is not known. The remaining rings correspond to other, less intense, reflections from either α-Fe, Fe_3O_4, or γ- Fe_2O_3.

The bright spots in the dark field photographs of Figs. 17-19 correspond to the iron crystallites diffracting into the objective aperture while imaging. The dark spots in the bright field photographs correspond to any crystallites causing diffraction of the electron beam out of the objective aperture.

Since the concentration of crystallites differ in the dark versus the bright field images for the deposits made at 300°C, quantitative information on the concentration of crystallites versus power is not possible without further experiments. Several qualitative conclusions may be made, however. First, the concentration of diffracting α-Fe crystallites increased from 200°C to 300°C. Second, the variation

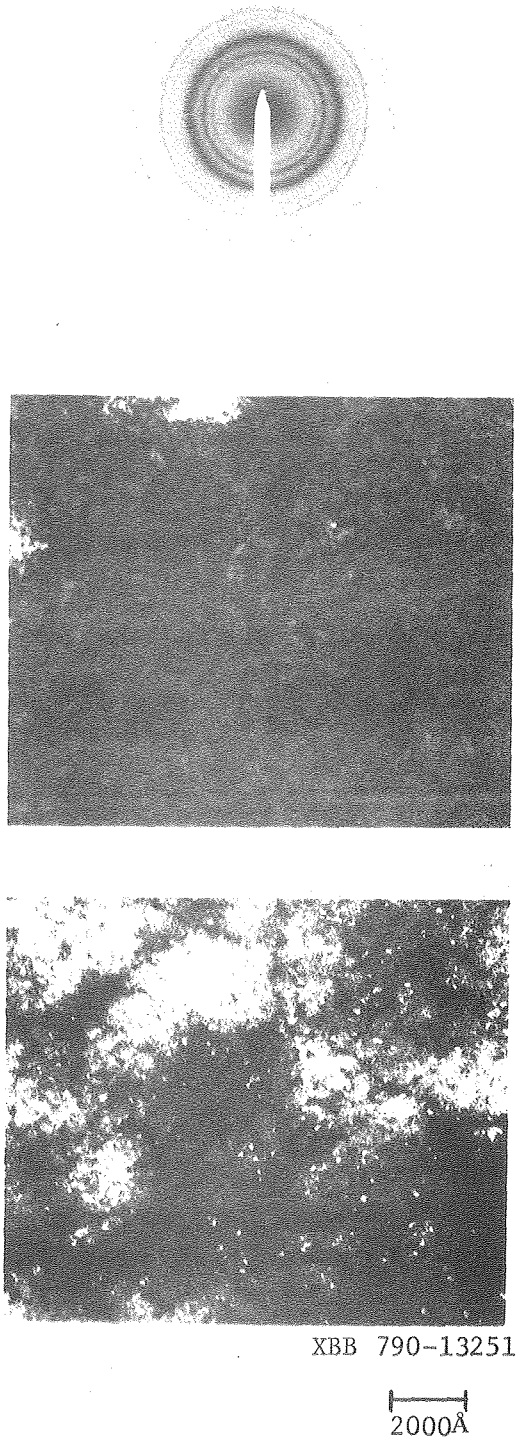

Fig. 17. Transmission electron micrographs for a film deposited onto NaCl at 200°C, 30 watts power. Top: electron diffraction pattern; middle: bright field; bottom: dark field.

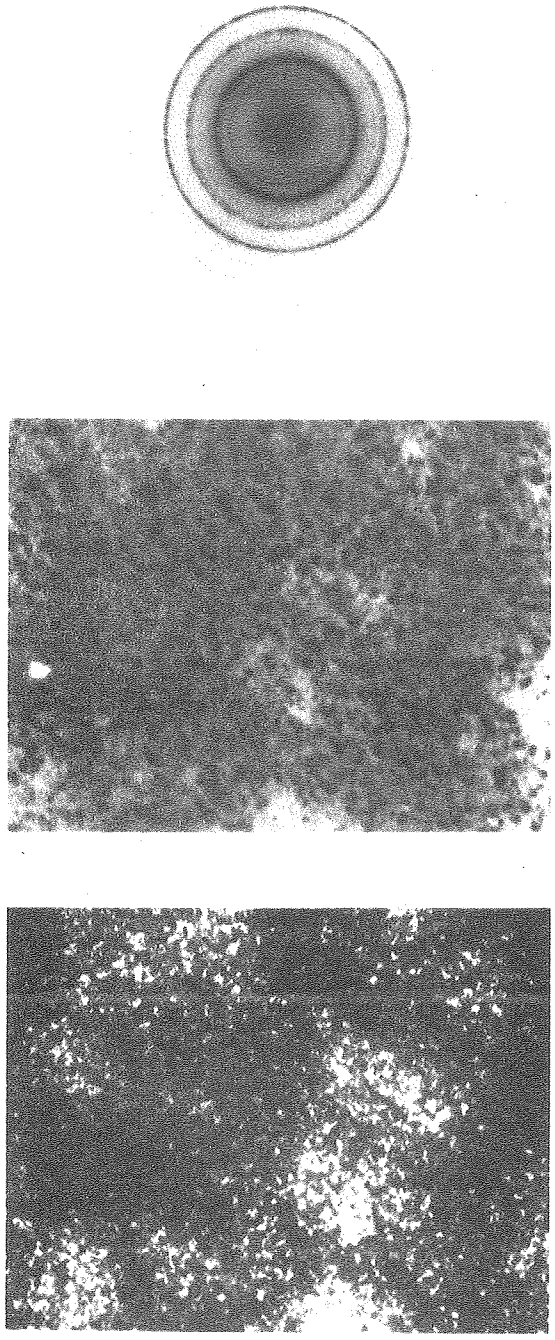

XBB 790-13250

2000Å

Fig. 18. Transmission electron micrographs for a film deposited onto NaCl at 300°C, 10 watts power. Top: electron diffraction pattern; middle: bright field; bottom: dark field.

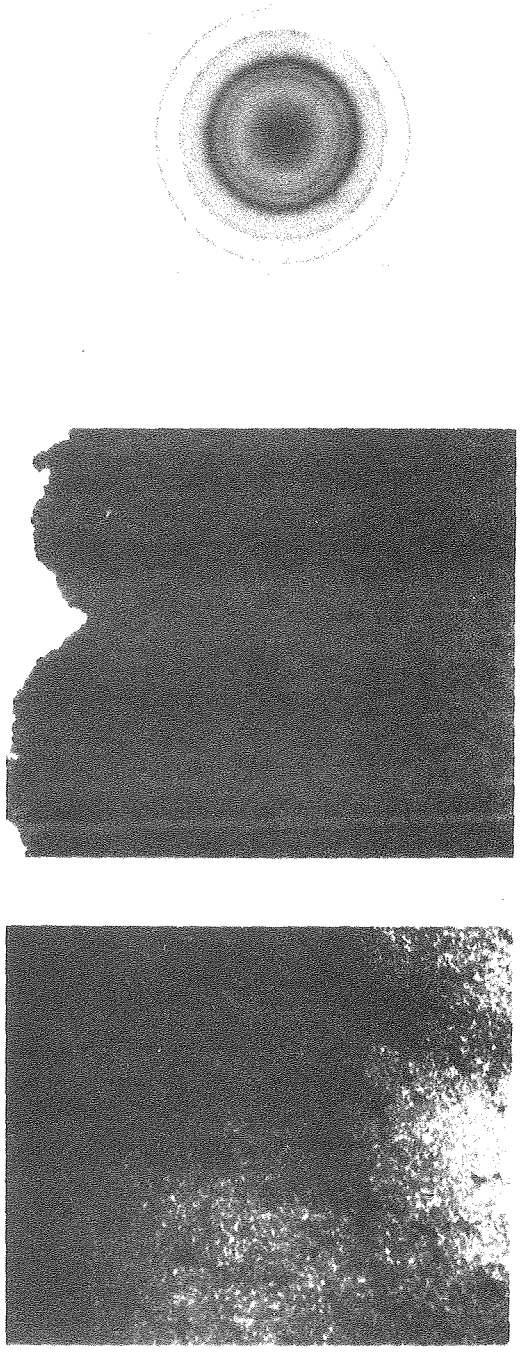

XBB 790-13249

2000Å

Fig. 19. Transmission electron micrographs for a film deposited onto NaCl at 300°C, 100 watts power. Top: electron diffraction pattern; middle: bright field; bottom: dark field.

of crystallite size was much greater at low than at high power levels. At 300°C and 10 watts power, crystallites ranging in size from 30 - 300Å were seen while at 300°C and 100 watts power many crystallites of a more uniform size of 70 - 140Å were observed. For comparison, the crystallite size observed at 200°C and 30 watts power ranged from 70 - 240Å. These observations support the hypothesis of crystallite damage (or decomposition) resulting from enhanced ion and electron bombardment at high power levels.

The small size of these crystallites also explains the rather broad x-ray diffraction peak observed at 2θ of 45 degrees (α-Fe). The increase in the concentration of crystallites with an increase in substrate temperature also explains the increasing intensity of the x-ray diffraction peak at 2θ of 45 degrees at increasing temperatures.

No quantitative information on the distribution and size of the iron oxide particles is possible without further experiments. Nevertheless, the presence of iron oxide diffraction rings in all cases implies the presence of iron oxide crystallites even at 200°C and 30 watts power where none was detected by x-ray diffraction (Fig. 14).

3. Surface Structure From Scanning Electron Microscopy

The surface microstucture was investigated with a Hitachi Model S-310A scanning electron microscope (SEM). The surface was quite smooth and uniform. Only at very high magnification (45,000X) was some structure observed. Four SEM photos are shown in Fig. 20. The feature size ranged from 200 - 1000Å. An increase in rf power from

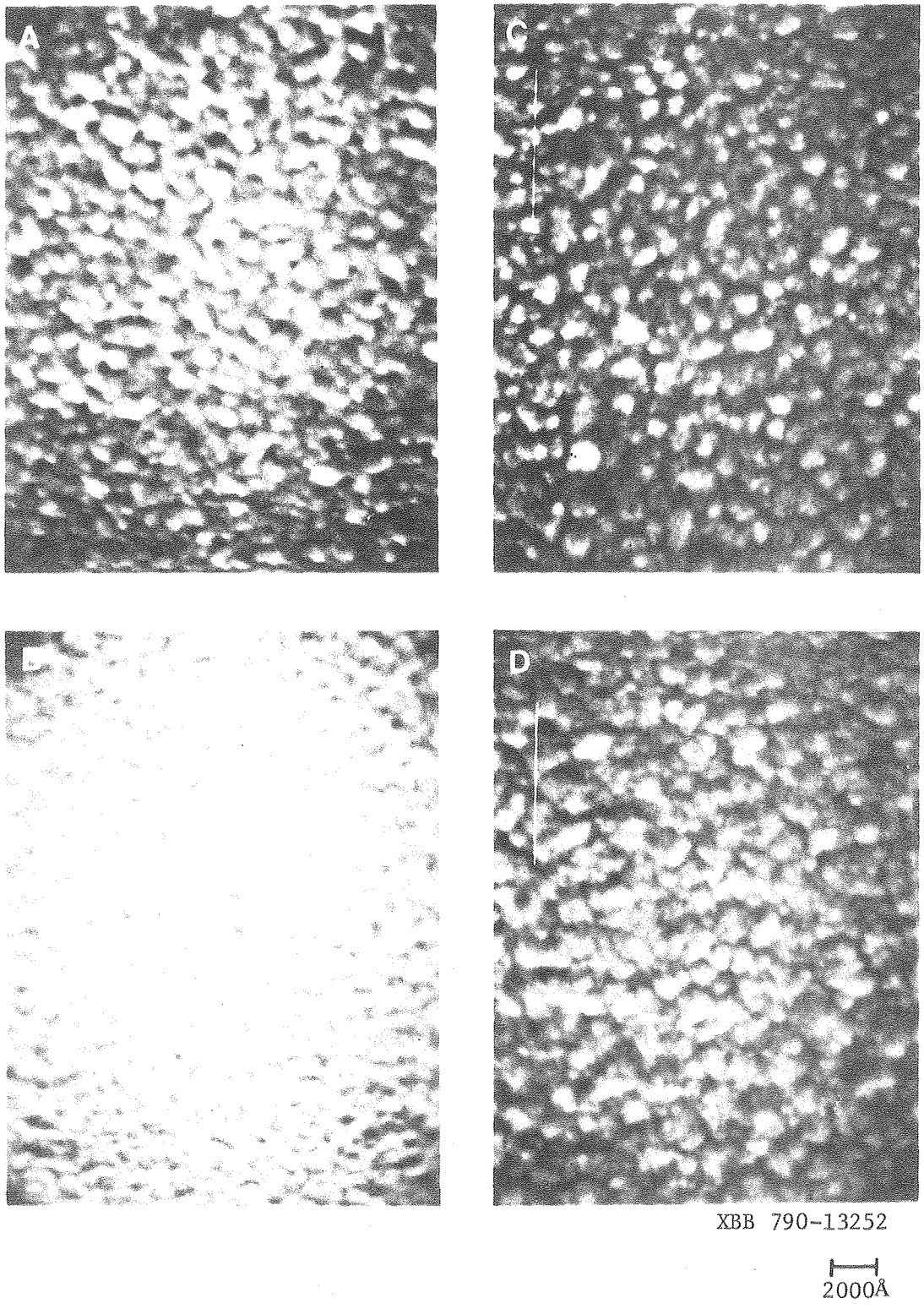

Fig. 20. Film surface structure from scanning electron microscopy. A: 300°C, 10 watts power; B: 300°C, 100 watts power; C: 200°C, 25 watts power; D: 200°C, 100 watts power.

10 to 100 watts at 300°C resulted in a more featureless surface, while little change was observed at 200°C as the power was increased.

It was not necessary to coat the samples with a conductor (to prevent charging) prior to observation with the SEM. The fact that little charging of the surface was observed, implies that the films are quite conductive. Some charging of surface particles does occur, however, as shown by the bright nodules (≈700Å diameter) in Fig. 20a. These results suggest that the bright nodules are crystallites of (nonconducting) iron oxide.

D. Magnetic Hysteresis

The magnetic hysteresis properties of the deposited films were investigated using the hysteresis looper described in Sec.II.A.2. Only when the magnetic field was applied parallel to the film plane was any hysteresis observed. The magnetization vector, therefore, was always in the direction of the film plane. This orientation is a result of the creation of large demagnetizing fields when $\vec{M}$ tilts out of the film plane thereby making nonparallel alignment difficult.[46]

The shape of the hysteresis loops varied widely depending upon the substrate temperature and rf power level. Two extreme examples are shown in Figs. 21-22. The loop obtained at 300°C and 100 watts rf power exhibited a much greater coercive force and loop squareness than was displayed by the film deposited at 200°C and 30 watts power. This trend was found to be true in general. The important hysteresis properties, namely the coercive force H_c, the loop squareness as given by the ratio of the remanent induction B_r to the saturation induction

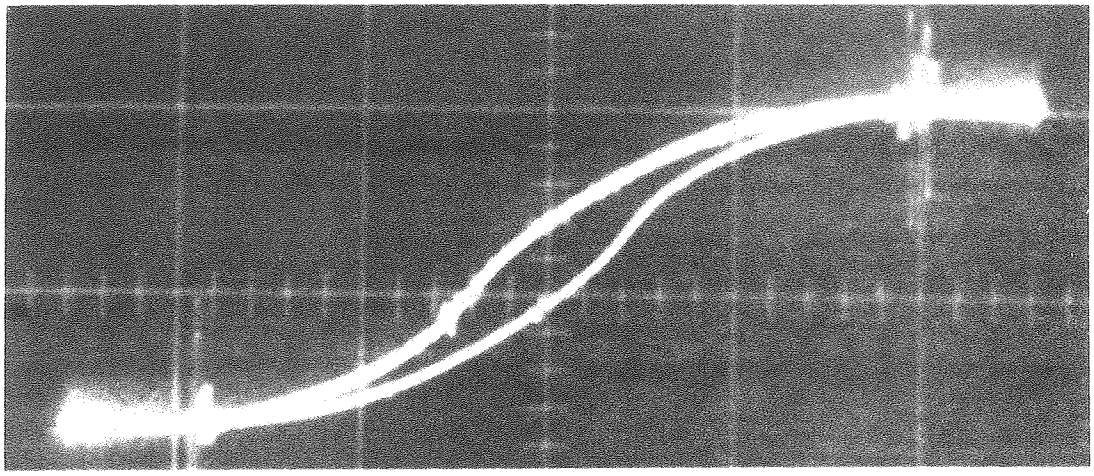

Fig. 21. The hysteresis loop resulting from a deposit run at 200°C and 30 watts power. (H_c = 6.60 oersted, B_r/B_s = .27, $\sigma_s = 1.5 \times 10^{-4}$ weber-meter/kilogram).

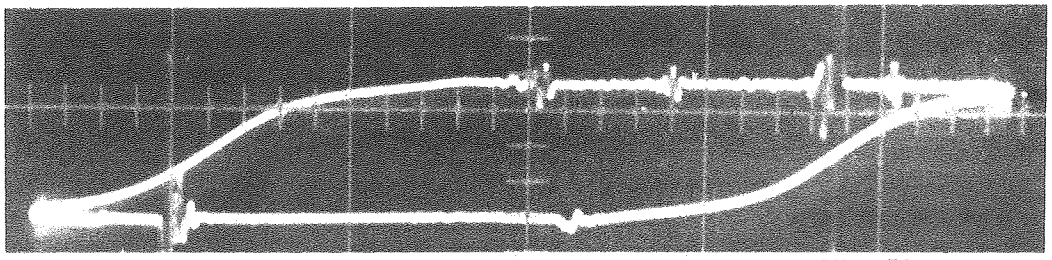

XBB 790-14173

Fig. 22. The hysteresis loop resulting from a deposit run at 300°C and 100 watts power. (H_c = 45 oersted, B_r/B_s = 1, $\sigma_s = 0.7 \times 10^{-4}$ weber-meter/kilogram).

B_s, and the specific magnetization at saturation (σ_s) are shown in Figs. 23-25 as functions of the rf power and substrate temperature.

At temperatures below 200°C no reproducible hysteresis loops were observed. These results are in agreement with the loss in crystallinity observed at temperatures below 200°C in the x-ray diffraction experiments and thus a loss or minimization of domain structure in the films.

At rf power levels above 10 watts at 200°C and at substrate temperatures above 200°C, definite trends were observed in the shapes of the hysteresis loops. First, the coercive force was found to increase with both increasing temperature and increasing rf power. Second, the loop squareness factor (B_r/B_s) increased with both increasing rf power and increasing substrate temperature. In fact, the deposits made at 300°C resulted in very square loops ($B_r/B_s \approx 1$) for power levels above 30 watts. Finally, the specific magnetization at saturation (σ_s) was found to decrease as the rf power increased.

The saturation induction, B_s, is mainly a function of the film composition and crystal structure.[40] An increase in B_s would be expected from an increase in iron content since it is the iron which exhibits the magnetic moment. The trend of decreasing σ_s (B_s/ρ) with increasing rf power correlates well with the decrease in iron content observed for increased rf power levels (see Fig. 10).

The coercive force, H_c, is a measure of the difficulty involved in moving the domain walls. The major impediments to domain wall motion are structural defects such as impurities, precipitates, or other crystalline imperfections.[1] An increase in coercive force may also be caused by a very small particle size (100 - 1000Å).[6] As pointed

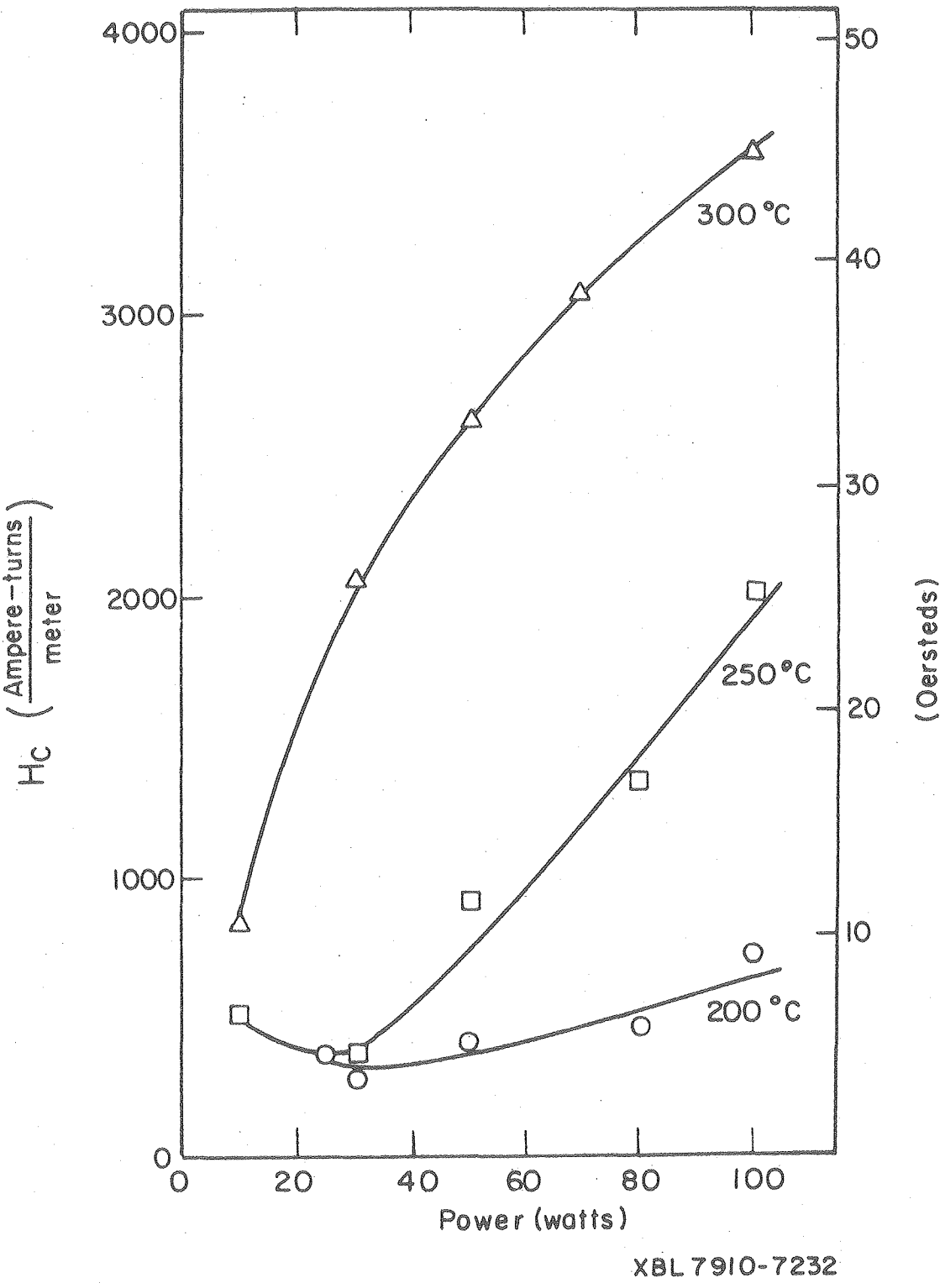

Fig. 23. The coercive force versus substrate temperature and rf power level.

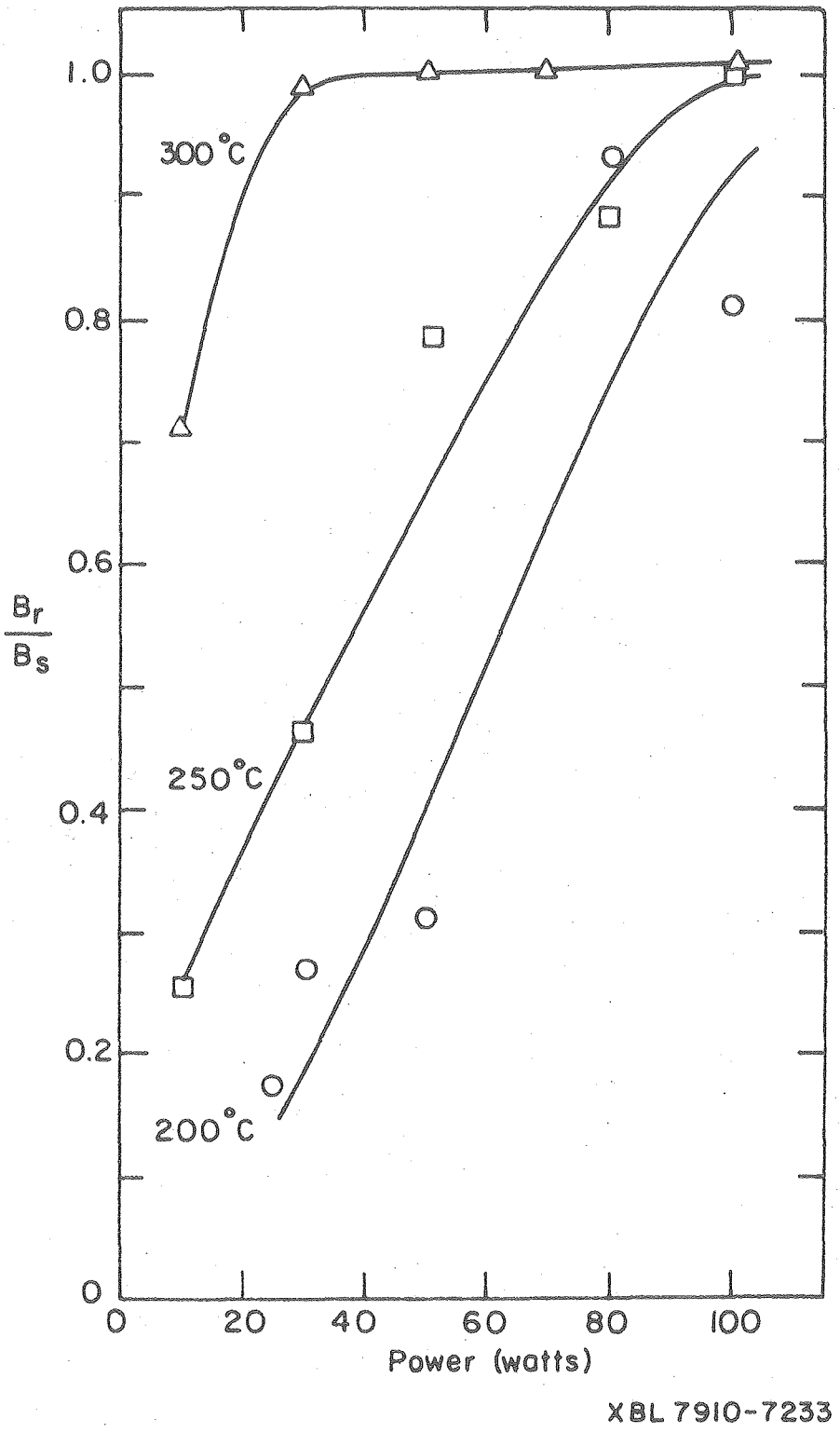

Fig. 24. The hysteresis squareness factor (B_r/B_s) versus substrate temperature and rf power level.

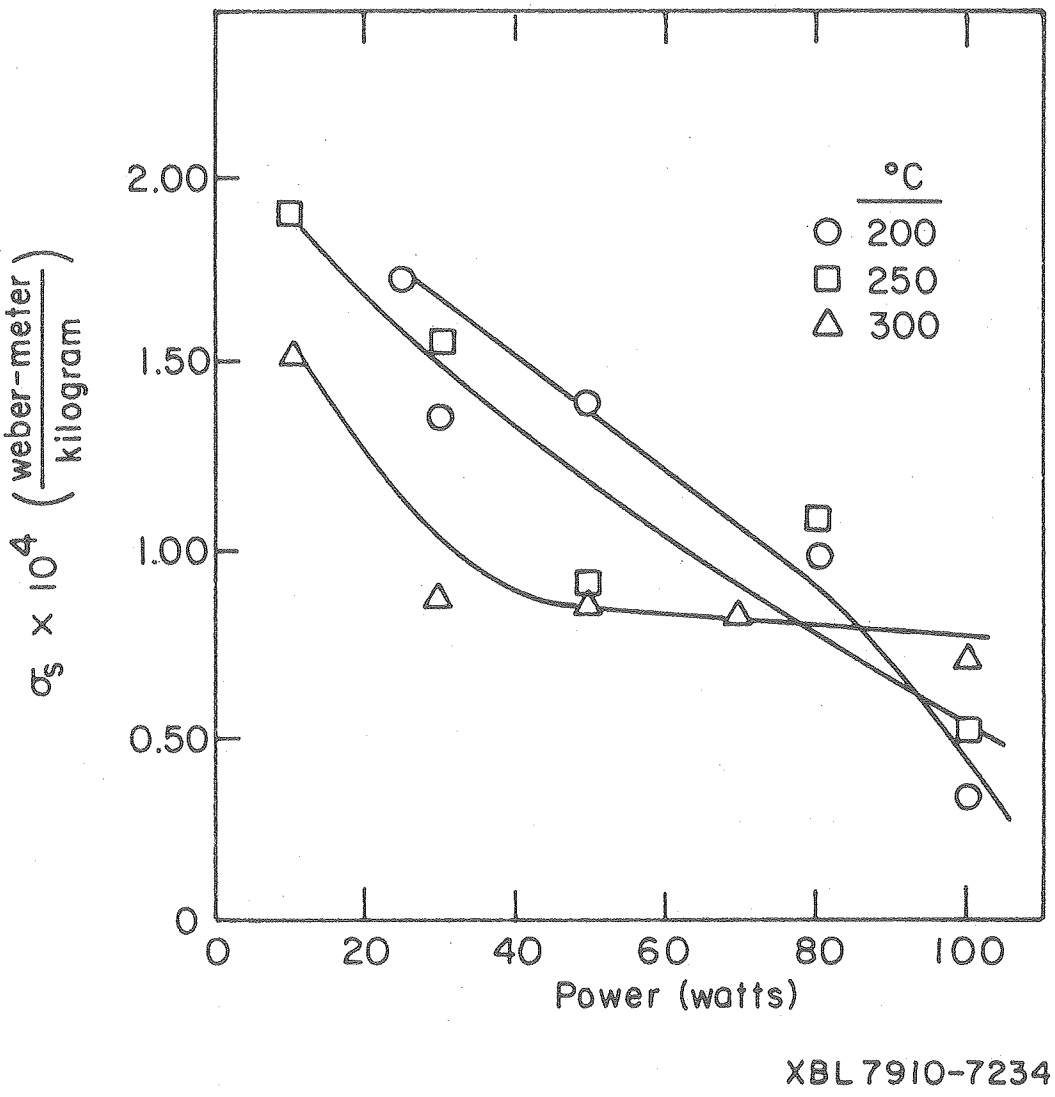

Fig. 25. The specific magnetization at saturation (σ_s) versus substrate temperature and rf power.

out in Sec. III.C.1. the decrease in intensity of the x-ray diffraction peak at 2θ of 45 degrees observed as the rf power was increased, was probably due to an increase in structural damage caused by increased ion and electron bombardment at high rf powers. This decrease in intensity could also be due to the marked increase in oxygen content found at increasing rf power levels. Both the increased structural damage and/or the presence of precipitates such as iron oxide could acount for the observed increase in coercive force with increasing rf power.

The coercive force was also found to increase as the substrate temperature was increased at rf power levels above 10 watts. The coercive force of evaporated iron films has been reported to increase with increasng substrate temperatures.[41] In Ref. 41 an increase in substrate temperature also resulted in an increase in grain size. It was not clear from the TEM studies (Sec. III.C.2.) that an increase in temperature also corresponded to an increase in grain size in the present experiments. However, the increase in temperature did increase the concentration of α-Fe crystallites greatly. No information on the distribution or size of iron oxide crystallites was obtained from the TEM experiments, but an increase in the concentration of iron oxide crystallites is consistent with the x-ray diffraction results. Thus, the increasing presence of iron oxide may explain the increasing coercive force as the substrate temperature was increased.

In these experiments, the coercive force ranged from 5 to 45 oersteds. Commercially pure iron has a coercive force of about 1 oersted.[42] Iron thin films (<1000Å), however, exhibit a wide range

of values for H_c (20 - 250 oersteds) depending upon the amount of oxidation, surface roughness, and film thickness.[45] Thus the range observed here for H_c is in general agreement with previous results obtained on iron films. In addition, the specific magnetization at saturation of bulk iron is 2.76×10^{-4} weber-meter/kilogram while that of magnetite (Fe_3O_4) is 1.17×10^{-4} weber-meter/kilogram.[47] Thus the results observed here of 0.3×10^{-4} to 1.8×10^{-4} weber-meter/kilogram are also in agreement with previous results reported on bulk iron and iron oxide.

E. Pressure Dependence

Preliminary work has been carried out on the effects of increasing pressure on the properties of the deposited thin films. A substrate temperature of 250°C was maintained while the pressure was increased from 26.6 Pa (.2 Torr) to 93.3 Pa (.7 Torr) by closing the throttle valve on the vacuum pump. The effect of closing the throttle valve was to increase the residence time of the gas species in the reactor thus increasing the pressure. The average electron energy was also decreased since the mean free path of the electrons is reduced at increased pressures.[48]

At a power level of 10 watts, an increase in pressure had little effect on the deposition rate. At 50 and 100 watts, however, the deposition rate was reduced by a factor of 3 as the pressure increased from 26.6 Pa to 93.3 Pa.

An increase in pressure had little effect on the diffraction patterns of the deposits run at 10 watts power. An intense peak was observed at 2θ of 45 degrees for pressures up to 93.3 Pa. This was

very similar in appearance to that shown previously in Fig. 15 (250°C, 10 watts power). At 50 and 100 watts power, no diffraction peak was observed at 45 degrees for pressures of 53.2 or 93.3 Pa while a small iron oxide peak at 2θ of 36 degrees was still observed at 100 watts rf power. The intensity of this peak (36 degrees) remained approximately constant with an increase in pressure from 26.6 to 93.3 Pa.

The change in pressure also had little effect on the iron content of the films deposited at 10 watts power. On the other hand, an increase in pressure reduced the iron content of the film deposited at 50 or 100 watts power. At 50 watts, the weight percentage of iron decreased from 86 percent at 26.6 Pa to 68 percent at 93.3 Pa. Similarly at 100 watts power, the weight percentage of iron dropped from 81.4 at 26.6 Pa to 69.7 at 93.3 Pa.

The magnetic properties of the films deposited at 53.2 or 93.3 Pa and 10 watts power were comparable to those reported earlier at a power level of 10 watts (see Sec. III.D.). At 50 and 100 watts, however, the reduced sample size at increasing pressures reduced the output signal to such an extent that no hysteresis loops were observed.

It is not clear why at 10 watts power the film properties were not affected by an increase in pressure yet at 50 or 100 watts both the deposition rate and crystallinity were drastically reduced with increasing pressure. This increase in pressure at high power levels was also accompanied by a reduction in iron content. Since no carbon analysis were made, the actual film stoichiometries are not known. An increase in oxygen content was observed earlier only with decreasing

temperatures or increasing power levels. An increase in pressure should not increase the rate of dissociation of carbon monoxide since the average electron energy has been reduced. Additional experiments are needed to further explain these observations.

IV. CONCLUSIONS

1. Plasma enhanced deposition can be used to form highly reflective, uniform, and adherent thin films of iron and iron oxide from an iron pentacarbonyl source.
2. The composition of the plasma deposited films was a strong function of the rf power level. As the rf power was increased more carbon monoxide was dissociated by the plasma into elemental oxygen and carbon, therefore incorporating more carbon and oxygen into the films. The increase in oxygen content was much greater than the carbon, however, for films deposited at substrate temperatures above 200°C.
3. Crystallites of α-Fe and iron oxide (Fe_3O_4 or γ-Fe_2O_3) were formed at substrate temperatures of 150°C or greater. The concentration of α-Fe crystallites increased with increasing temperature. The size of these α-Fe crystallites ranged from 30 - 300Å (300°C, 10 watts power) to 70 - 140Å (300°C, 100 watts power) to 70 - 240Å (200°C, 30 watts power). The intensity of the α-Fe x-ray diffraction peaks decreased with increasing rf power. Therefore, the concentration of α-Fe crystallites also appeared to decrease with increasing rf power, although this has not yet been confirmed by TEM. Increasing electron and ion bombardment and the increase in oxygen content of the films observed at high rf power levels can explain this reduction in the concentration of α-Fe crystallites. The increase in oxygen content at increased power levels also resulted in increased iron oxide formation.

4. The thin films exhibited magnetic hysteresis when deposited at temperatures above 150°C. The coercive force and the loop squareness factor increased with both increasing substrate temperature and increasing rf power levels. The formation of more iron oxide at increasing temperatures or increased rf power levels can explain the observed increase in coercive force. The specific magnetization at saturation also decreased as the rf power increased. This trend correlates well with the decrease in iron content observed at increasing rf power levels. Finally, the magnetization vector always remained in the plane of the film due to the creation of large demagnetizing fields when $\vec{M}$ tilted out of the film plane.

ACKNOWLEDGMENTS

I would like to express my appreciation to the director of my research, Professor Dennis W. Hess, for his professional advice and guidance during my graduate study.

I also thank Dr. Raja K. Mishra for his help and advice in this work.

This work was supported by the Division of Material Sciences, Office of Basic Energy Sciences, U. S. Department of Energy under Contract Number W-7405-ENG-48.

REFERENCES

1. R. Rose, L. Shepard, and J. Wulff, "Electronic Properties" in Volume IV of "Structure and Properties of Materials," Wiley, New York, 1966, p. 223.
2. A. Bobeck, P. Bonyhard, and J. Geusic, Proc. of the IEEE, 63 (8), 1176 (1975).
3. J. Mallinson, Proc. of the IEEE, 64 (2), 196 (1976).
4. J. Freedman, IEEE Trans. on Magnetics, MAG-5 (4), 752 (1969).
5. Ref. 1, p. 209.
6. C. Kittel, "Introduction to Solid State Physics," 5th edit., Wiley, New York, 1976, p. 484-492.
7. M. Prutton, "Thin Ferromagnetic Films," Butterworths, Washington, 1964, p. 4.
8. R. Soohoo, "Magnetic Thin Films," Harper and Row, New York, 1965, p. 5.
9. M. Francombe, Trans. of the 10th Natl. Vac. Symp., 316 (1963).
10. N. Schwartz, Trans. of the 10th Natl. Vac. Symp., 325 (1963).
11. E. Kay, Adv. Electron., 17, 245 (1962).
12. E. Kay, J. Appl. Phys., 32 (3), 99S (1961).
13. M. Rand, J. Vac. Sci. Technol., 16 (2), 420 (1979).
14. R. Rosler, W. Benzing, and J. Baldo, Solid State Technology, June 1976, p. 45.
15. D. Carlson and C. Wronski, Appl. Phys. Lett., 28, 671 (1976).
16. H. Kobayashi, M. Shen, and A. Bell, J. Macromol. Sci.-Chem., A8 (2), 373 (1974).
17. A. Bell, J. Vac. Sci Technol., 16 (2), 418 (1979).

18. A. Bell, Solid State Technology, April 1978, p. 89.

19. R. Kirk, "Applications of Plasma Technology to the Fabrication of Semiconductor Devices" in "Techniques and Applications of Plasma Chemistry," J. Hollahan and A. Bell, eds., Wiley, New York, 1974.

20. J. Hollahan and R. Rosler, "Plasma Deposition of Inorganic Thin Films" in "Thin Film Processes," J. Vossen and W. Kern, eds., Academic Press, New York, 1978.

21. Par Lauriat, J. Appl. Cryst., 9, 175 (1976).

22. D. Secrist and J. MacKenzie, Ceramic Bulletin, 45 (9), 784 (1966).

23. Ref. 8, p. 148.

24. Ref. 7, p. 74.

25. H. Oguey, Rev. Sci. Inst., 31 (7), 701 (1960).

26. B. Cullity, "Elements of X-Ray Diffraction," 2nd. ed., Addison-Wesley, Reading, Massachusetts, 1978, p. 188.

27. "Powder Diffraction File," JCPOS International Center for Diffraction Data, Swarthmore, Pennsylvania (1978).

28. H. Willard, L. Merritt, and J. Dean, "Instrumental Methods of Analysis," 5th. ed., D. Van Nostrand Co., New York, 1974, p. 350-381, 791-793.

29. J. Finegan and R. Hoffman, Trans. Natl. Vac. Symp., 8, p. 935-42 (1961).

30. H. Murbach and H. Wilman, Proc. Phys. Soc. B66, 905 (1953).

31. H. Carlton and J. Oxley, A. I. Ch.E. Journal, 11, 79 (1965).

32. L. Brown and A. Bell, Ind. Eng. Chem., Fundam., 13, 210 (1974).

33. F. McTaggart, Aust. J. Chem., 17, 1182 (1964).

34. F. McTaggart, "Plasma Chemistry in Electrical Discharges," Elsevier, New York, 1967, p. 217.

35. M. Roberts, Trans. of the Faraday Soc., 57, 99 (1961).

36. D. Davies and U. Evans, J. Chem. Soc., London, 4373 (1956).

37. L. Collins and O. Heavens, Proc. Phys. Soc., 70 (3-B), 265 (1957).

38. B. Cullity, "Elements of X-Ray Diffraction," 2nd. ed., Addison-Wesley, Reading, Massachusetts, 1978, p. 140.

39. J. Coburn and H. Winters, J. Appl. Phys., 50, 3189 (1979).

40. Ref. 6, p. 466.

41. L. Reimer, Z. Phys., 148, 527 (1957).

42. R. Bozorth, "Ferromagnetism," Van Nostrand Co., New York, 1951, p. 54.

43. Ref. 42, p. 243, 246.

44. Ref. 7, p. 256.

45. Ref. 7, p. 93.

46. M. Cohen, "Ferromagnetic Properties of Films" in "Handbook of Thin Film Technology," L. Maissel and R. Glang, eds., McGraw-Hill, New York, p. 17-11.

47. National Research Council, "International Critical Tables of Numerical Data, Physics, Chemistry, and Technology," Vol. 6, McGraw-Hill, 1929, p. 376, 413.

48. A. Bell, "Fundamentals of Plasma Chemistry" in "Techniques and Applications of Plasma Chemistry," J. Hollahan and A. Bell, eds., Wiley, New York, 1974, p. 12.

49. B. Chapman, J. Vac. Sci. Technol. 11, 106 (1974).

50. C. Melliar-Smith, J. Vac. Sci. Technol. 13, 1008 (1976).

51. S. Clark, Jr., ed., "Handbook of Physical Constants," Geological Society of America, 1966, p. 80, 89, 90, 95.

TECHNICAL INFORMATION DEPARTMENT
LAWRENCE BERKELEY LABORATORY
UNIVERSITY OF CALIFORNIA
BERKELEY, CALIFORNIA 94720